POLITECNICO
DI TORINO

Master Degree Course in Biomedical Engineering

DET - Department of Electronics and Telecommunication

Master Degree Thesis

Novel system for detection of pattern reversal visual evoked potentials

Supervisors:
Prof. Eng. **Danilo Demarchi**
Eng. **Alessandro Sanginario**

Candidate:
Giacomo Amela

July 2018

Abstract

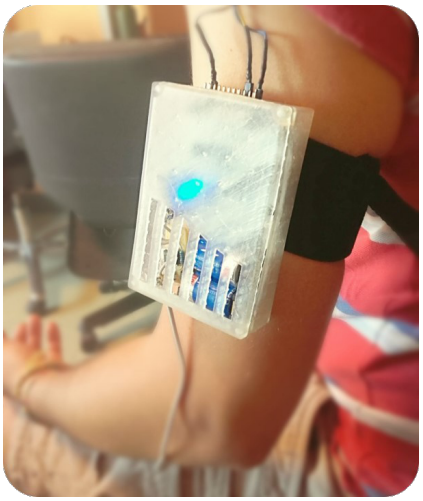

OBJECTIVE: The purpose of this work is to create a low-cost portable diagnostic instrument in ophtalmology, particularly aimed at the investigation of a signal called *pattern reversal visual evoked potential* (pr-VEP), in order to replace, at least in the first steps of the evaluation of the patient, the commercial instrument (Retimax® CSO).

MATERIALS AND METHODS: Epson Moverio BT-200 Smart Glasses are used to generate the pattern reversal stimulus. Electroencephalographic signal, taken through 3 electrodes positioned following the 10/20 international system, is acquired by a commercial acquisition card (OpenBCI® Cyton board) and is sent via bluetooth to a PC. Here, through a Matlab® algorithm, the data are processed and filtered appropriately in real time, dividing them in epochs of length equal to the time window of stimulus of the reversal pattern and making the average between the epochs obtained.

STATISTICAL ANALYSIS AND RESULTS: After having set up the system introduced a year ago [1], a recalibration was done on 10 healthy subjects, then a preliminary validation on 11 pathologic subjects, for a total of 42 eyes analyzed. To evaluate its functionalities, the 10 features that characterize the three main waves have been extrapolated from the signal (amplitudes and latencies of N75, P100, N135, amplitudes and relative latencies N75-P100 and N135-P100) and a non-parametric analysis was carried out on them, using various algorithms such as the Kolmogorov-Smirnov test, the scatter plot, the Bland-Altman plot and comparing the averages of the data obtained with the Retimax and the Smart Glasses. Finally, a purely visual evaluation was made, overlapping the signals acquired by the two systems in the same graph.
The results show an excellent correlation between the data obtained from healthy subjects and a good correlation between the data obtained from the pathological subjects. In the near future the device will be tested on a large scale and it will be improved at level of hardware and software.

Contents

List of Figures

List of Tables

Chapter 1

Introduction

1.1 Sensory Information

The approach to the study of sensations dates back to the nineteenth century with Weber and Fechner's researches on sensations psychophysics. They found out that, despite the differences of sensations they produce, all the sensory systems, when properly stimulated, relay signals sharing four basic attributes of stimulus informations, i.e. *modality*, *site*, *intensity* and *time course*.

The *modality* defines a general class of stimuli based on the type of energy that they transmit. The receptors, together with the central pathways connected with them and the brain areas involved, make up the sensory systems and the nervous system generates specific types of sensations, like touch, taste, sight and hearing.

The *site* of stimulus is represented by all the receptors of a sensory system that are activated.

The *intensity* of stimulus is defined by the amplitude of the response of every receptor, which is related to the amount of stimulus energy released at the level of the receptor itself.

The *time course* of the stimulus is established by the beginning and the end of the receptor's response and depends on the speed at which the stimulus energy begins to be effective and ends up being at the receptor level. [10]

1.2 Overview of anatomy and ocular physiology

The eye is a sense organ which has the task to transduce visual electromagnetic waves into electric signals (Figure 1.1).
The ocular bulb is composed of three tunics: an external or *fibrous* one, a medium or *vascular* one and an internal or *nervous* one. These three tunics form together the wall of the ocular globe. The nucleus of the ocular bulb consists instead of *aqueous humor*, *lens* and *vitreous humor*.
The *fibrous* tunic represents the protective envelope of the eye; it consists of two parts in continuity with each other: the sclerotic or *sclera*, which constitutes the 2/3 posterior and the *cornea* anteriorly.
The *vascular* or chorionic tunic is the medium shade of the eye, which continues forward giving rise first to the *ciliary body* and then to the *iris*, a membranous disk with a central hole called *pupil*. This vascular lamina not only plays an important trophic function but also collaborates with the visual function: it has in fact a layer of pigmented cells that, together with the retinal pigment epithelium, absorbs the light rays that have passed through the retina and prevents reflection on the sclera. From the ciliary body the *zonular fibers* start to attach themselves to the *lens* of the eye, placed behind the iris and at the level of the ciliary body. These two structures participate in a complex process that is *accommodation*.
A photosensitive layer extends to the choroid, the *retina*, which terminates anteriorly at the level of the *ora serrata*, that is the junction between the choroid and the ciliary body. It contains the photoreceptors of the eye responsible to the conversion of the light stimulus into electrical potential.[11][12]

Within the eye we can distinguish three chambers: an anterior chamber between the cornea and the iris; a posterior chamber between the iris and the crystalline lens; a vitreous chamber located behind the lens.
The first two chambers contain the *aqueous humor*, a transparent liquid produced by the ciliary body that flows through the *Schlemm canal* into the

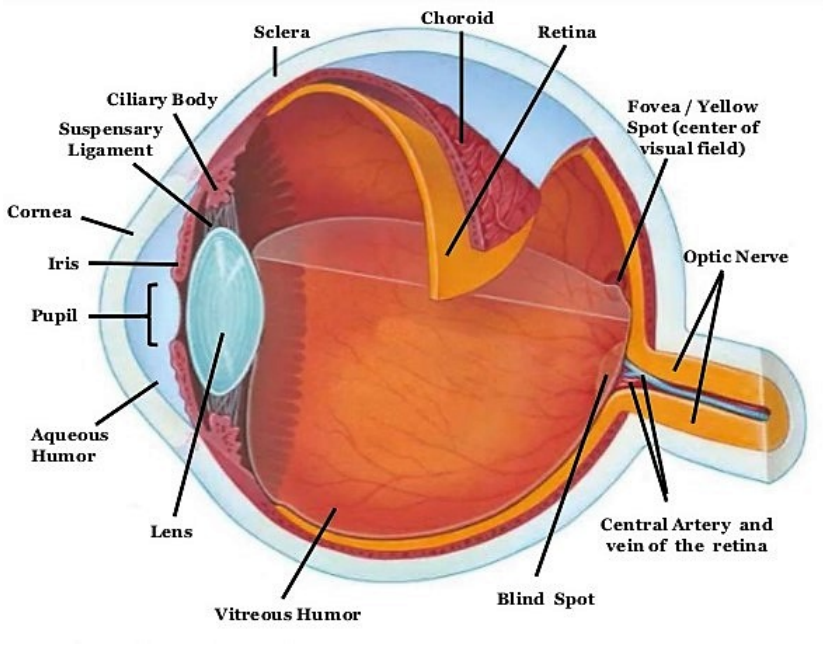

Figure 1.1: *Principal components of the human eye. [2]*

scleral veins, while the vitreous chamber is occupied by the *vitreous body*, a gelatinous mass that helps determine the shape of the eyeball occupying 2/3 of the volume.[11][12]

By focusing on the photosensitive portion of the eye, we know that the retina is made up of nerve cells organized into ten layers (Figure 1.2). The photoreceptors, which as previously mentioned, act as transducers of the light signal, are distinguished in *cones*, concentrated mainly in the *fovea centralis* (area of greatest visual acuity at the center of the *macula*) and *rods*, located in the remaining portions of the retina.
[13] Photoreceptors via amyelin axons contract synapses with *bipolar cells*; these in turn, through nerve fibers that run on the inner surface of the retina, make contact with the *ganglionic* or *multipolar* neurons, whose neurites converge towards the *optic papilla*, nasally placed at the macula and devoid of receptors, to form the optic nerve. At this point the axons are coated with myelin sheath.[14]

Each of the two halves of the retina, nasal and temporal, receives light

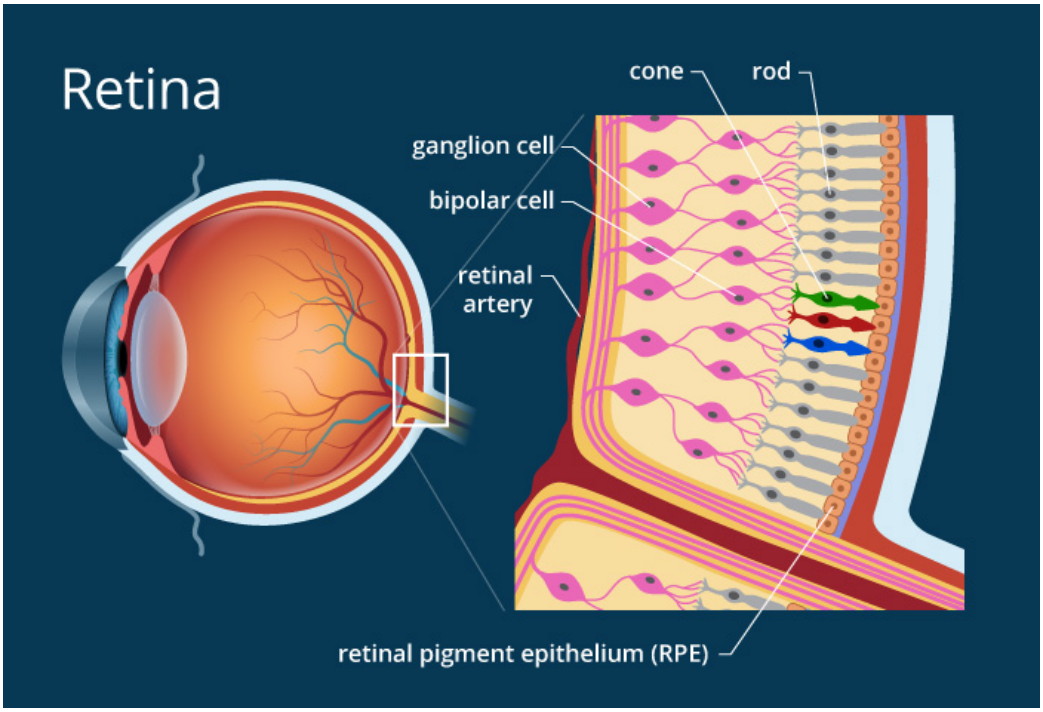

Figure 1.2: *Structure of the retina. [3]*

stimuli from the opposite half of the visual field. In the optic nerve fibers are placed in distinct bundles: fibers of the macula (central area of the nerve), temporal fibers (lateral area), nasal fibers (medial area), fibers of the lower quadrants and of the upper quadrants. The optic nerve, emerging from the optic papilla, leaves the eyeball and passes through the *optical hole*.
Once in the anterior cranial fossa, the two optic nerves join in the *optic chiasm*. At this level the fibers coming from the nasal half of the retina intersect themselves and go in the *contralateral* optical tract, while the fibers coming from the mid-temporal are brought into the *ipsilateral* optic segment without crossing. In this way each visual hemi field projects into the contralateral hemisphere. The optical traits carry the visual information to the *lateral geniculate body*, in which the fibers undergo a 90° rotation in the medial direction. Shortly before reaching the lateral geniculate body a contingent of fibers detaches from the distal third of the optic tract to move into the upper necks and the nuclei of the pretectal region of the midbrain, representing the afferent pathway of the nervous arch for the photomotor reflex.

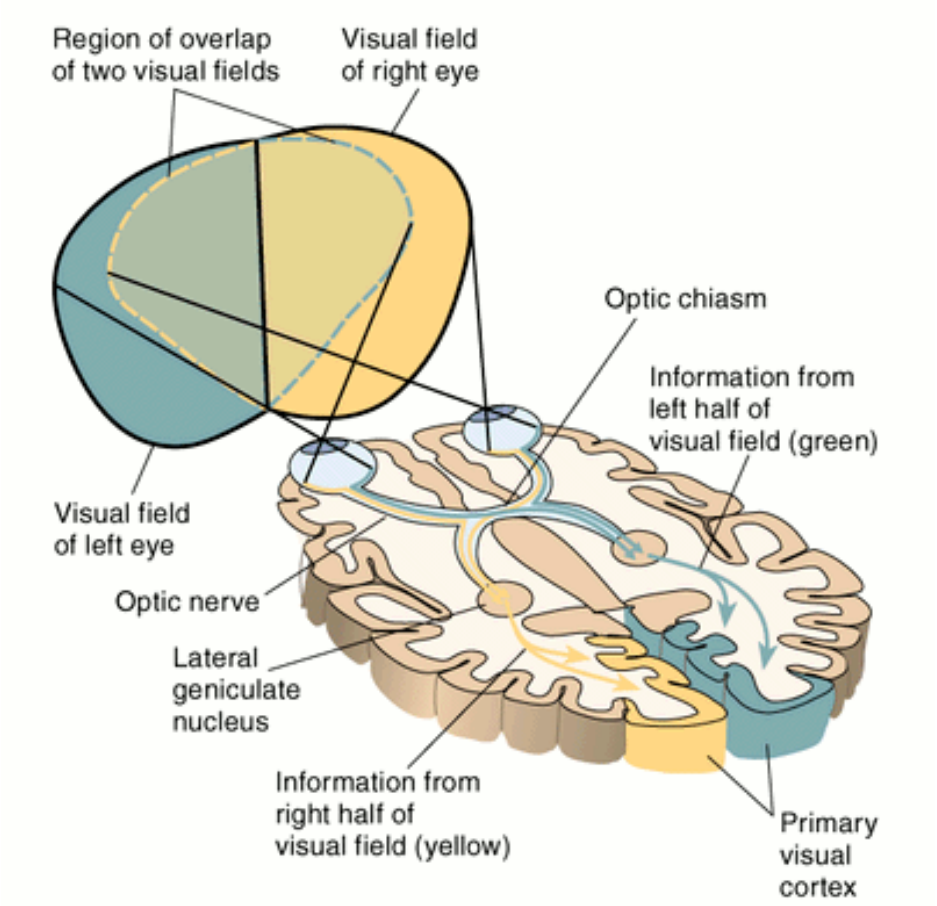

Figure 1.3: *Visual Pathways. [4]*

[15][16] From the lateral geniculate body the optical radiations originate, divided into upper bundle (lower part of the parietal lobe containing the fibers coming from the upper part of the retina) and lower bundle (temporal lobe, fibers coming from the inferior retina). The optical radiation reaches the *striated occipital cortex* (primary visual area): at the upper lip of the *calcarial fissure* the fibers coming from the upper retinal quadrants terminate, while at the lower quadrants the lower ones terminate (Figure 1.3). [17][16]

As all the information necessary to recreate an image on a cerebral level passes through the optic nerve and the nervous pathways described above, every small alteration can cause serious damage to the view. Regardless of the cause, the most common symptoms referable to an optic nerve pathology are: [18]

- Reduction of visual acuity with the possibility of reaching up to complete blindness;
- Dyschromatopsia;
- Alterations of the visual field (scotomata, hemianopsis, quadrantopsias);
- Pain (if there is an inflammatory substrate).

Faced with these symptoms, for the purposes of a correct diagnostic classification, it is essential to perform the following investigations: [18]

1. Anamnesis;
2. Evaluation of visual acuity;
3. Examination of the fundus oculi;
4. Perimetric or campimetric examinations;
5. Study of eye movements by means of an electrooculogram (EOG);
6. Evaluation of the retinal morphology and of the optic nerve by OCT (Computerized Optical Tomography) and RM (Magnetic Resonance);
7. Electrofunctional investigations (ERG, F-ERG, mfERG, PERG, PEV).

1.3 Electrofunctional tests

Electrofunctional tests allow to study the bioelectric activity of the optic nerve and of the retina (Figure 1.4).

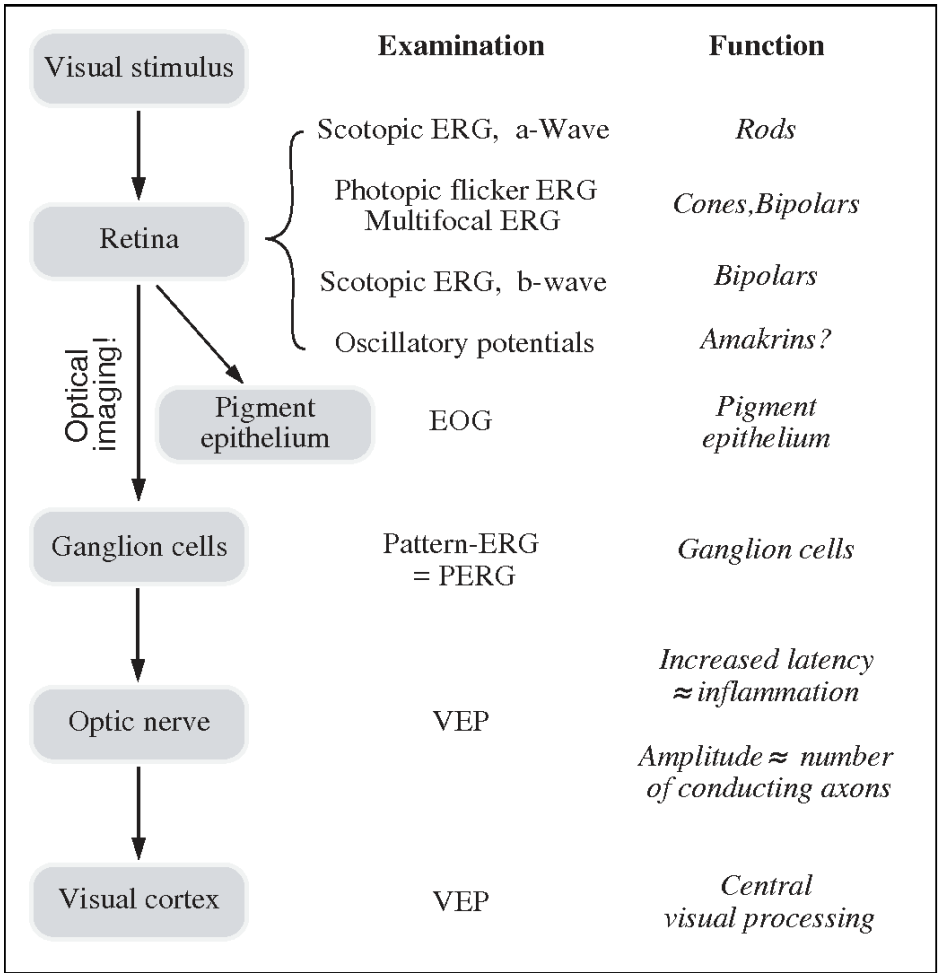

Figure 1.4: *Various types of examinations referred to the anatomical part that they analyze. [5]*

Currently it is possible to make an objective evaluation of the functionality of the different elements that form the optical pathways through different -and specific- tests:

a. **Standard electroretinogram (ERG)**: also called *flash* ERG, it is an electrofunctional test that evaluates the bioelectrical retinal response to

an unstructured light stimulus (flash). Flash ERG allows in particular to test the functioning of the most external retinal layers (pigment epithelium, photoreceptors, bipolar cells and amacrine cells) and it is characterized by a series of alternating polarity waves, among which we recognize the wave a, the wave b and the oscillator potentials. [19]

b. **Focal electroretinogram (F-ERG)**: also called *foveal* ERG or *focal macular* ERG, it is mainly used to evaluate the macular function of the cones. The number of cones located in the 10th centrals represents about 7% of the total cone population and 2% in the fovea. The responses of the standard ERG generated by the macular cones represent therefore just under 10% of the total contribution of cones, which explains the usefulness of the F-ERG in detecting a dysfunction limited to the macular region. [20]

c. **Multifocal electroretinogram (mfERG)**: it allows to isolate the electrical response of the macular region by simultaneously recording the signal from multiple retinal areas within the central 40°. MfERG is used in cases in which the deficits of central visual function are not associated with visible changes in the retina under examination of the ocular fundus, in which the standard ERG is normal. The multifocal ERG also arises to compensate for a lack of the F-ERG: the focal ERG responses can not monitor the measurement (area) of the macular dysfunction and the response does not provide any differentiation between the photoreceptors and the internal cells of the retina. [21]

d. **Pattern electroretinogram (PERG)**: retinal biopotential generated by a temporally modulated pattern stimulus and constant total luminance (typically grid or chessboard). The PERG was born to study the activity of ganglion cells; in fact, the optimal stimulus for these cells is most often represented by a chessboard with alternating presentation (reversal). In this way the background retinal illumination remains constant and a traditional flash ERG is not recorded.[22]

e. **Visual Evoked Potentials (VEP)**: see the next section.

1.4 Visual Evoked Potentials

VEPs are evoked electrophysiological potentials that can be extracted from the cortico-registered electroencephalographic activity after visual stimuli [6]. The acquisition of these signals provides information on the integrity of the nerve conduction pathways, from the retinal photoreceptors up to the occipital cortex.
Their genesis can be traced back to two components: a primary one, originating from the activity of retinal photoreceptors, which reaches the occipital area through the lateral geniculate ganglion and a secondary one that reaches the cortex from the retina through the reticular substance [23].

There are two main types of PEV, which are characterized by different types of stimulus:

- **Flash VEP** (luminance variation stimulus);
- **Pattern VEP** (contrast variation stimulus).

Flash VEPs are visual evoked potentials recorded after stimuli consisting of a stroboscopic flash, with the possibility to change the light intensity and the frequency of the flashes. Until the 1970s almost all of the registered VEPs were of this type. Flash VEPs reflect the global macular functioning of the photopic system and the condition of its signal along the macular visual pathways, up to the primary visual areas. The flash visual evoked potentials consist of a series of positive and negative waves, which can be displayed in a range between 30 and 300 ms (Figure 1.5) [7].

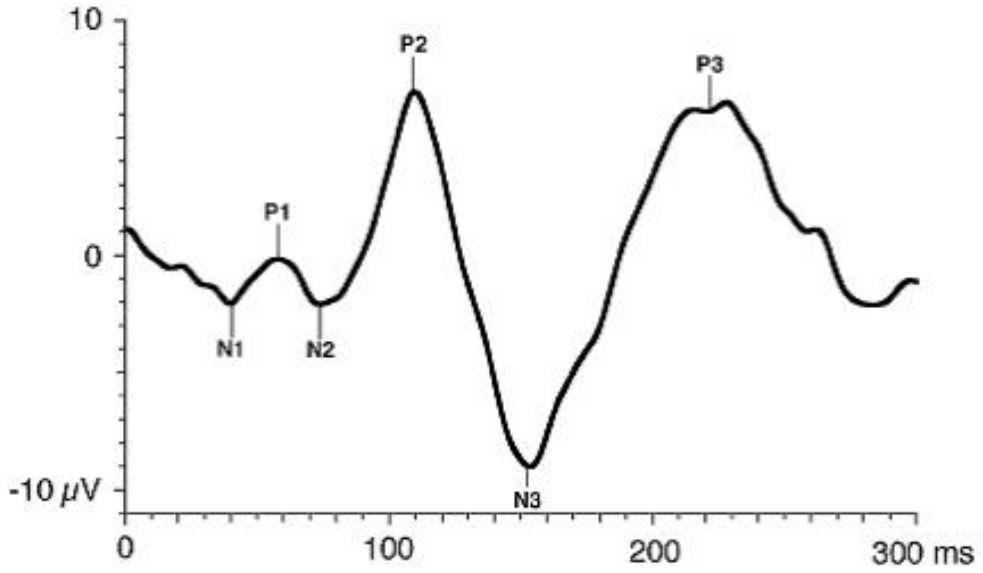

Figure 1.5: *Typical morphology of a flash VEP: you can see all the main waves that characterize the path of an healthy subject. [6]*

However, this type of VEP has two important disadvantages in clinical application:

1. Great physiological variability in the response;
2. Substantial insensitivity in the presence of visual function disorders.

For this reason today it is poorly used; however, it remains the most suitable electrodiagnostic test in patients with severe reduction in visual acuity, children or non-cooperating subjects and patients in coma state.

In 1959 Barlow suggested that the different types of cortical neurons require specific visual patterns in order to produce the maximum response. On the basis of these considerations the contrast stimuli that characterize the patterned VEPs have been realized.
These are periodic images with a geometrically oriented structure, whose contrast is modulated while keeping the overall brightness constant [24].

This type of stimulation is perfectly suited to the physiological requirements of the high resolution retinal areas (*fovea*) and therefore promotes a functional exploration of a specific optic nerve fiber contingent. Pattern stimulation can consist in replacing structured elements with a neutral background without changes in total brightness (*onset / offset pattern*), or in a complete alternation of one element per unit area (*pattern reversal*) [7].
The *on / off pattern* technique can be useful in the discovery of a disease simulation and in patients with nystagmus. The response to pattern on / off stimulation consists physiologically of three major peaks in adults, located in a range between 75 and 150 ms (Figure 1.6).

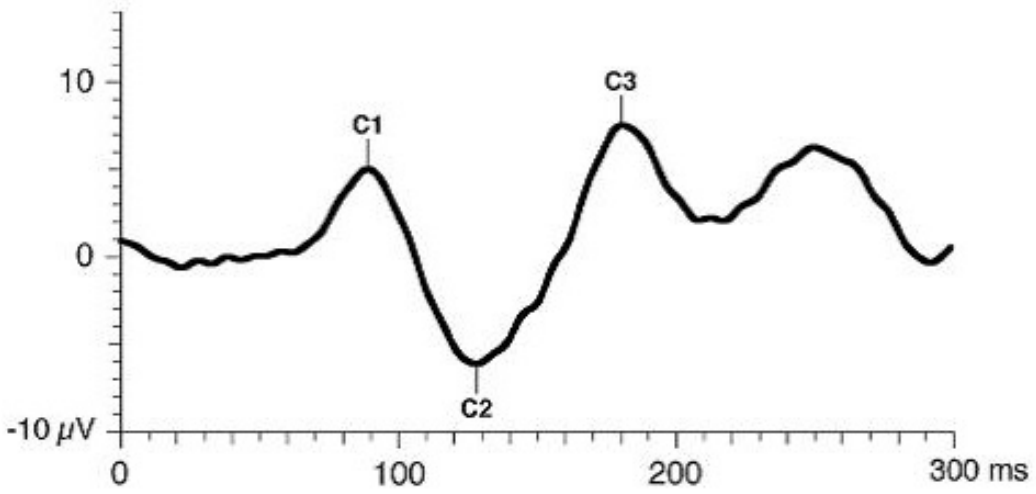

Figure 1.6: *Typical morphology of an on / off pattern VEP: you can see the three principal waves that characterize the path of an healthy subject (C1, C2, C3). [7]*

The *reversal pattern* is the most used technique for most of the clinical purposes: this is the reason that led us to analyze it more in depth and that has convinced us to focus our project on this type of pattern.
Its stimulus consists of a chessboard that changes phase (the white squares become black and vice versa) suddenly and repeatedly with a specific number of inversions per second [7].
The stimulus should have well-defined characteristics:

a. The diameter of the view field should exceed 15 degrees in its narrowest dimension;

b. The inversion rate should be within 1-3 inversions per second;

c. The brightest element on the screen should have luminance greater than 80 cd/m^2 , while the luminance average of all the elements should be greater than 40 cd/m^2.

d. The single element (a square of the chessboard) should have a contained size in the range of 15-60 minutes of arc;

e. Image contrast should exceed 75%.

Pr-VEP is characterized by three main waveforms, whose nomenclature consists in describing the polarity, followed by the typical average peak latency (Figure 1.7):

1) **N75**: negative peak visible at about 75ms from the stimulus;

2) **P100**: positive peak visible at about 100ms from the stimulus;

3) **N135**: negative peak visible at about 135ms from the stimulus.

While it is well established that the N75 wave originates at the level of the primary cortex (V1), the genesis of P100 and N135 waves is still controversial [23].
Some researchers have suggested that P100 is primarily generated in extrastriate visual areas, while others agree that P100 (like N75) is generated in the striated cortex. Finally, as regards the wave N135, while some studies have identified the source in the extrastriate visual areas, others conclude that this component originates from the calcarine cortex or from both striata and extrastriata areas [23].
Most of the authors agree that this uncertainty in the origin of the VEP can be partially explained by the fact that the various studies on the subject have

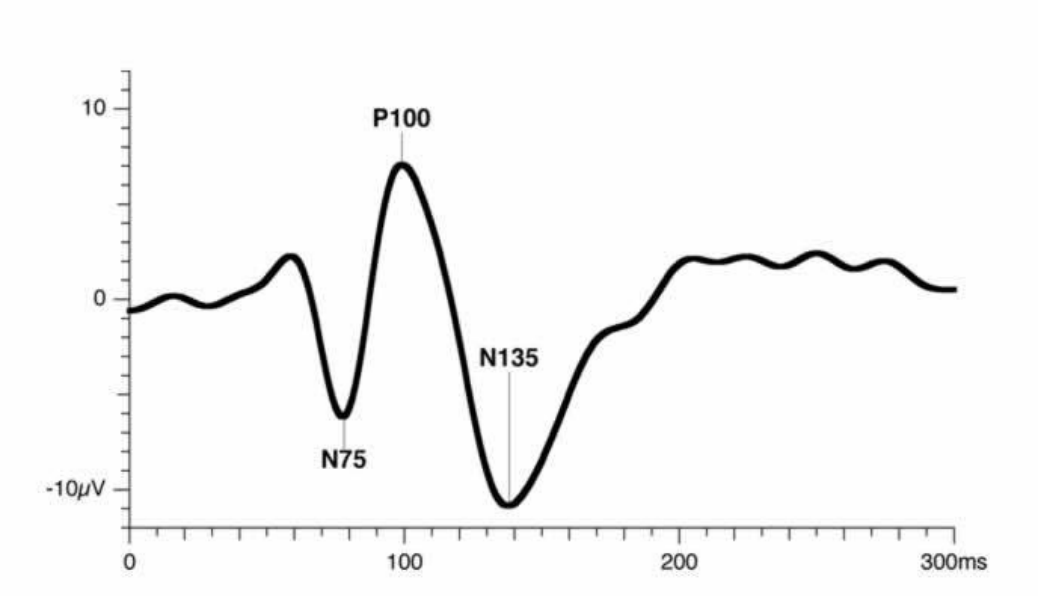

Figure 1.7: *Typical morphology of a pattern reversal VEP: you can see the three principal waves that characterize the path of an healthy subject (N75, P100, N135). [7]*

adopted different types of stimulus as well as different techniques of signal analysis [23].

Although VEPs present a precise morphological characterization, they are influenced by some factors such as the temporal frequency of the stimulus and the patient's age.
The types of VEP described above are the only ones covered by the ISCEV Standardized Protocol; there are many other types of non-standardized VEPs, characterized by different stimuli, even if they are less used [6]:

- Steady State VEP;
- Sweep VEP;
- Motion VEP;
- Chromatic VEP;
- Binocular VEP;

- Stereo-elicited VEP;
- Multi-channel VEP;
- Hemi-field VEP;
- Multifocal VEP;
- Multi-frequency VEP;
- LED Goggle VEP.

1.5 Pattern Reversal VEP Interpretation

The anomalies of VEPs are not specific and may concern a wide variety of ophthalmological but also neurological pathologies. At the time of interpretation it is necessary to relate the data collected, with the normative ones. The principal parameters that must be taken into account, in order to determine if the answer is normal or not, are the follows:

1. Latency of the P100 wave;
2. Width of the P100 wave (that is measured from the peak of the N75 wave);
3. Latency interval between N75 and N13 waves;
4. Latency difference between the P100 waves of right and left eye.

What you get can be:

- "*Extinct*" or "*non-recordable*" VEP, when the answer is not identifiable or when the recorded tracks are not repeatable;
- "*Hypovolted*" VEP, in which a reduction in amplitude is highlighted;

- VEP "*with delayed latencies*", in which there is an increase in latency;
- "*Hypovolted and with delayed latencies*" VEP, in which there are changes in amplitude and latency;
- "*Asymmetric*" VEP, in which there is an increase in the interocular latency difference. [25]

An example is given by the Figure 1.8:

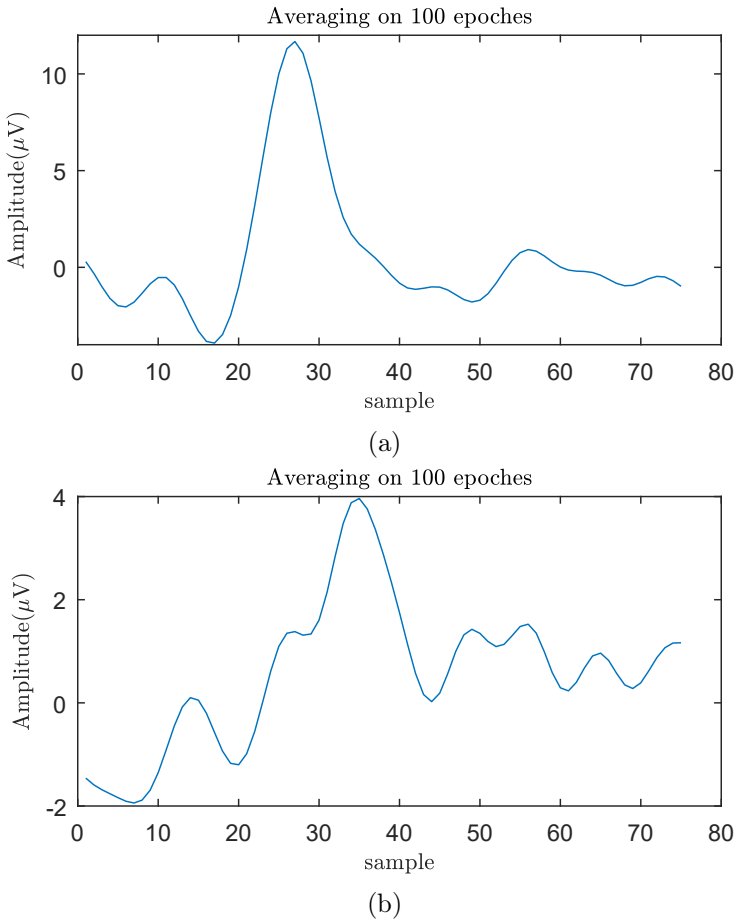

Figure 1.8: *A comparison between an healthy (a) and a pathologic VEP plot (b). In this case the pathologic VEP belongs to the class of the "Hypovolted and with delayed latencies VEP": in fact you can see an increase of the P100 amplitude and a latency delay.*

1.6 Clinical Application

Pattern reversal VEPs have a high sensitivity in detecting anomalies which are present throughout the visual system. Depending on the pathology, pr-VEP can signal e.g. the presence of demyelination phenomena, expressed by changes in latency and increase in retinal-cortical conduction time, or indicate the existence of axonal damage, evidenced by changes in amplitude and morphology of the answers.
The pathologies in which this type of diagnostic test can be used are the following [25]:

- Multiple sclerosis;
- Parkinson's disease;
- Leukodystrophies;
- Migraine;
- Maculopathy;
- Glaucoma;
- Ischemic optic neuropathies;
- Leber optic neuropathy;
- Idiopathic intracranial hypertension;
- Toxic-nutritional diseases;
- Atassie (Friedreich).

This study is focused on maculopathy for three main reasons:

1) Frequency of the disease: maculopathy affects many more patients and therefore it is of greater interest for a clinical trial than other eye conditions. Moreover it is easier to find them;

2) High sensitivity of VEP for the aforementioned disease: 90% of the photoceptors responsible for the signal, in fact, are found in the central portion of the retina (macula), that's why a pathology located in that stretch of the optical pathways could be immediately identified [13];

3) Reduced variability among different subjects: the response to the prvep of a maculopathic subject is much more standard compared to subjects with other diseases.

1.7 State Of Art

One of the currently device used for diagnostic test of Patter Reversal VEP and chose for this study is Retimax CSO. Compliant with the ISCEV standard [7], Retimax CSO, in its various forms, is a device dedicated to recording bioelectrical responses; objective and non-invasive, the device analyzes dysfunctions of retinal ganglion cells before the apoptosis process begins.
Retimax CSO allows to detect retinal dysfunctions of the central 20-40 degrees of the retina [26].

There is no doubt that it is an useful and innovative device for the early diagnosis of important eye diseases, but we have to consider that there are some limitations, including the high cost (about 25 thousand euros) and the non-portability, due to the number and the large size of its various components.
The need of a portable, economical and equally accurate device was the starting point of the study conducted in [1] and the final aim of this thesis.

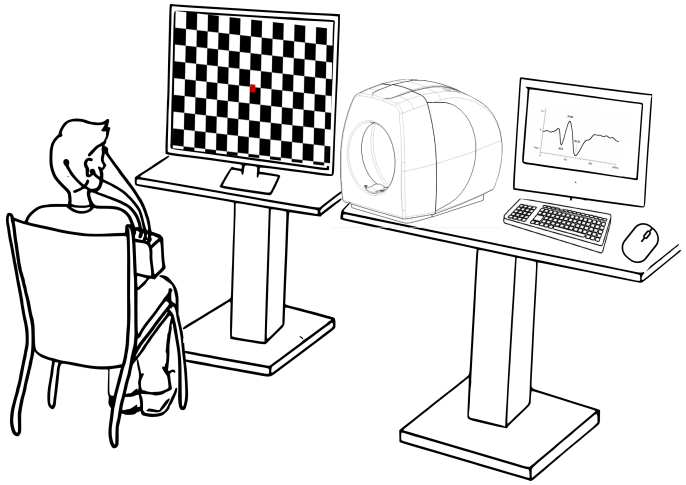

Figure 1.9: *A representation of the entire system while it is working.*

1.8 Purpose of the study

As I said before, the study aims to create a portable, handy and economical instrument, but equally accurate in identifying the signal in question, both in healthy subjects and in pathological subjects.

Before my inclusion in the project, the device had a stimulation system and an acquisition system. The acquisition system was composed of a commercial acquisition board and a dongle bluetooth connected to the pc. The stimulation system consisted of a pair of Smart Glasses, an ArduinoOne board and an hc-06 bluetooth module, connected to the Arduino (Figure 1.10).
Through the MATLAB ® GUI, hc-06 bluetooth module sent the input to Smart Glasses, which, through an Android app, began to display the reversal-pattern (two images that alternate every 500 ms). MATLAB® algorithm started to process the data making the average between the free-artefacts-epochs; every epoch was finally re-aligned with a template through the Spectral Matching algorithm (Figure 1.11).

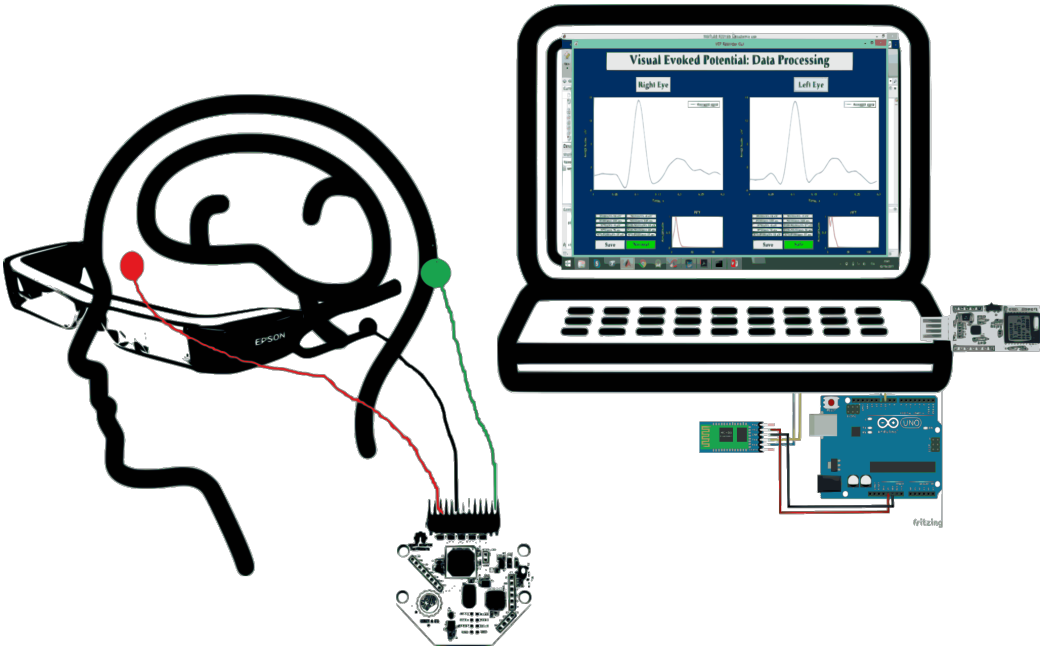

Figure 1.10: *The system conceived in [1]: this was the configuration before my inclusion in the project.*

The problems we had to face were the following:

1. The hc-06 bluetooth module, connected to the ArduinoOne board, generated a random delay when the input was sent to the stimulation system, which led to an error in the timing of the epochs;

2. The Spectral Matching algorithm realigned the various epochs with a synthetic template; as a consequence an error of clinical evaluation could be induced, because the information on the latency of the waves that characterize a VEP signal was completely lost.

To solve these problems, first of all I had to correct the defects found and improve the functionality of the device, and then perform a new calibration on healthy subjects; after that the device was tested on consenting pathological subjects at the "Sperino" ophthalmic center, in Turin.

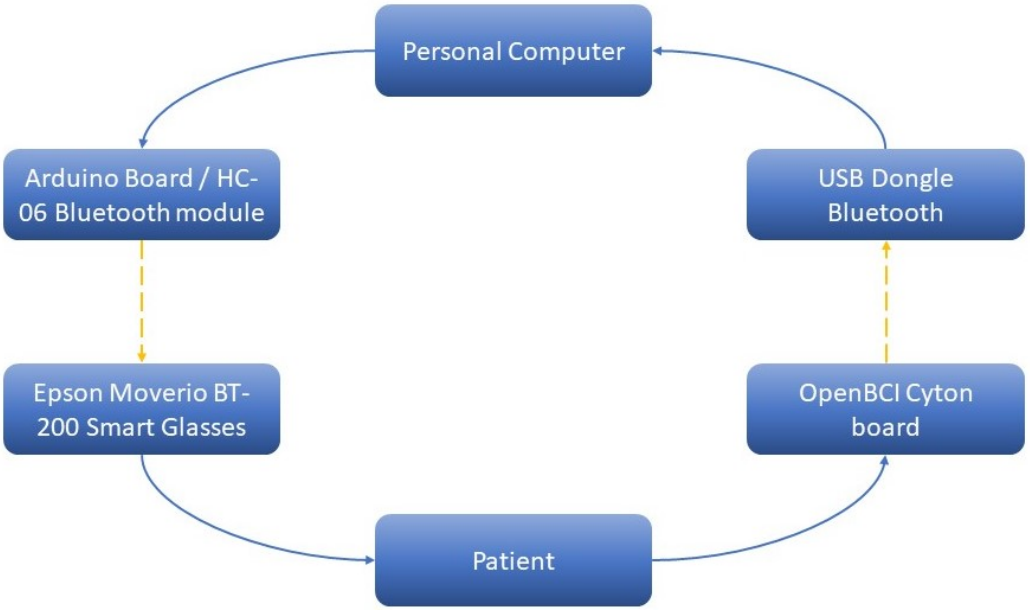

Figure 1.11: *Block diagram of the operation of the old system: the blue continuous lines indicate a cable transmission, while the yellow dotted lines indicate a bluetooth transmission.*

Chapter 2

Materials and Methods

2.1 Retimax CSO

The Retimax system, in its various versions, is composed of (Figure 2.1):

1. Isolation transformer for powering the whole system;
2. Flash stimulator of light with varying intensity or bright light alternating on a precise visual angle under the visible light spectrum;
3. Two-channel preamplifier, able to detect electric biopotentials generated by the retina and occipital visual cortex, with galvanic isolation of the patient, a CMRR of 110 dB and a 10 Ω input impedance;
4. Stimulator for the presentation of structured image on a television screen;
5. Computer where the signal analysis system is installed;
6. Monitor for printing biopotential graph.

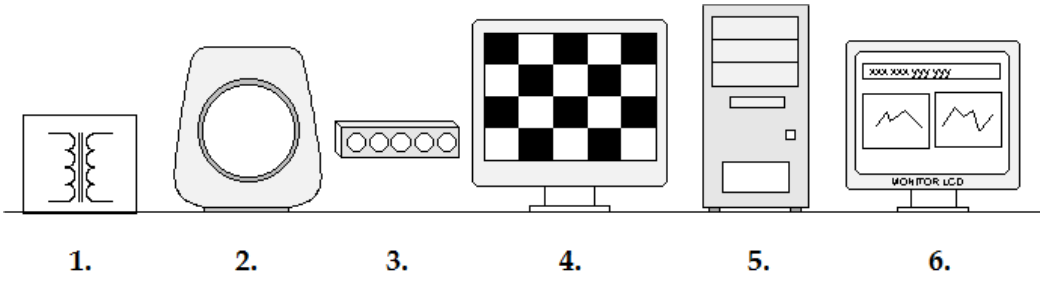

Figure 2.1: *The various parts of the Retimax CSO.*

Other accessory tools used in combination with Retimax CSO during the examination are:

a. Nuprep Skin Gel for effectively lowers impedance: abrasive gel for improving conductivity and helping achieve efficiency with the equipment; [27] (Figure 2.2a)

b. Ag/AgCl EEG Gold Skin Electrodes "SKIN CUP" with connecting cables; [28] (Figure 2.2b)

c. KONIX EEG Paste: it allows the correct application of the electrodes on the skin, limiting the electrode-skin impedance. [29] (Figure 2.2c)

(a) (b) (c)

Figure 2.2: *Three needed accessories for the VEP test.*

2.2 Epson Moverio BT-200

The device in question consists of a pair of smart glasses and an external controller connected to the glasses.
The Epson Moverio BT-200 smart glasses (Figure 2.3a) are not medical devices, but they provide important performances and are equipped with a large number of technological features (that can be exploited in this area as well). In fact, the Moverio BT-200 boasts a 1.2 GHz dual core processor and 1 GB of RAM; the battery has up to six hours of battery life, the internal memory is 8 GB and is expandable by an additional 32 GB via SD card [30]. As for connectivity, these smart glasses have a Wi-Fi connection (compatible with smartphones and tablets), Bluetooth and USB. The Moverio BT-200 is equipped with a miniaturized projection system based on the Ultimicron HTPS panels (high polysilicon TFT LCD panels) used in 3 LCD projectors. The screen has an aspect ratio of 16: 9, a resolution of 960x540 pixels for each of the three LCD layers and a refresh rate of 60 Hz. The screen size is comparable to a 40-inch screen located at a distance of 2.5 meters, while the field of vision covers about 23 degrees. The projection of the lenses is independent but it allows the brain to process a single three-dimensional image [8].

The external controller (Figure 2.3b) is equipped with an Android 4.0.4 operating system controlled by a touchpad and some basic buttons (on / off, home and return) and is an ideal platform to fully exploit the potential of augmented reality, as it is possible to use the kit SDK standard for app development.
Finally, these smart glasses are very comfortable, light (about 88 g), easy to use and cost about 600 dollars [8].

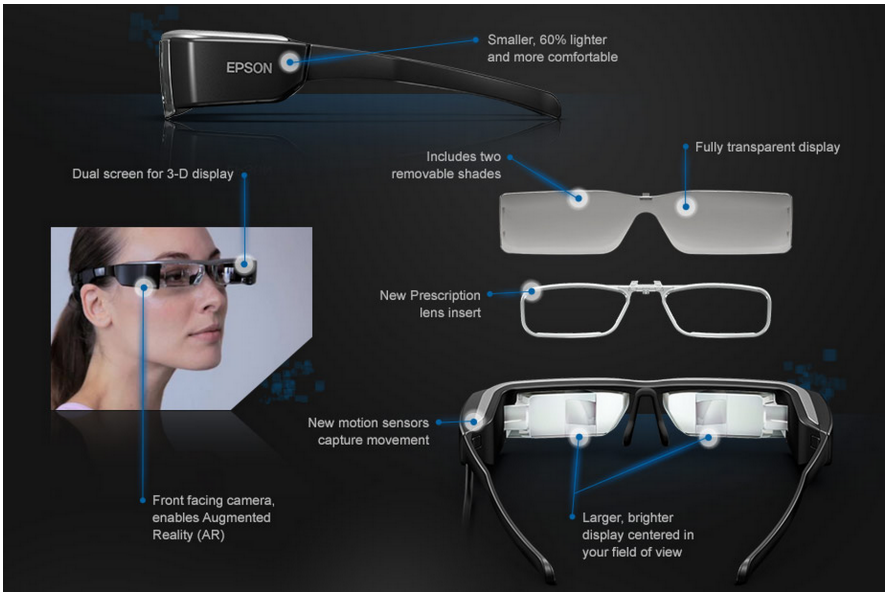

(a)

(b)

Figure 2.3: *Some features of the two parts of the system: figure (a) represent the Smart Glasses, while figure (b) shows the external controller [8].*

2.3 OpenBCI Cyton Board and OpenBCI Dongle

The OpenBCI Cyton board, unit to the relevant Bluetooth Dongle, constitutes the device acquisition system. The board mounts a 32-bit processor, to which the PIC32MX250F128B microprocessor is added; It has 8 data transmission channels and is arduino-compatible [9] (Figure 2.4).
Other important features are:

- Sampling frequency of 250 Hz;
- Programmable gain (seven pre-set levels from 1 to 24);
- 3.3 – 12 V input voltage;
- Micro SD card slot;
- 5 GPIO pins, 3 of which can be analog;
- 6 V power supply.

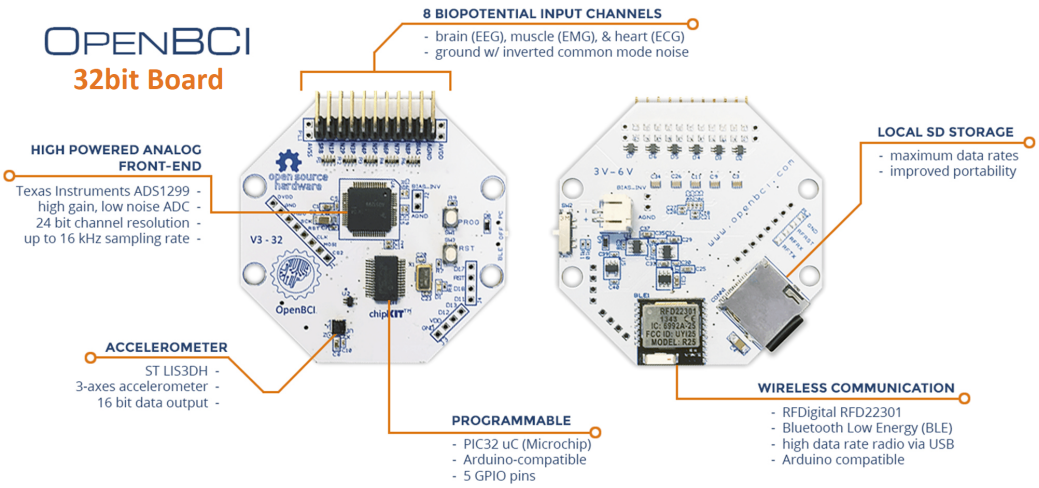

Figure 2.4: *Open BCI Cyton board: structure and features [9].*

The board communicates with the PC through the USB Bluetooth Dongle, connected to the latter, using RFDuino radio modules (Figure 2.5). It

can also communicate with other devices (tablets and smartphones) through the "bluetooth low energy" (BLE) mode. The dongle establishes a serial connection with the computer's on-board FTDI chip [9].

Figure 2.5: *OpenBCI Dongle Bluetooth [9].*

2.4 Secondary Instruments

During the development of the device, performed at the "Pierluigi Civera" laboratory of the DET (Department of Electronics and Telecommunications) at the Politecnico di Torino, some secondary tools were used, in order to detect problems and improve its functioning:

- **NIDAQ USB-6259**: A high-speed multi-function data acquisition DAQ module optimized for higher accuracy at high sample rates. The instrument has 32 Analog Inputs, 48 Digital Inputs / Outputs and 4 Analog Outputs and has a resolution of 16 bits (Figure 2.6);
- **Signal generator**;
- **Oscilloscope**;
- **Voltage generator**.

Figure 2.6: *NIDAQ USB-6259*

2.5 Hardware and Software's Improvements

Above mentioned in paragraph 1.8, the device had two main problems: one related to the hardware component of the system, which caused a random delay preventing the correct timing of the epochs and one related to the post-processing of the acquired signal, which prevented a correct reading of the signal.

To solve this problem we took some different steps:

1. At first, we presumed that the delay could be related to a poor accuracy of the synchronization system. We introduced a push button connected to both the Arduino board and cyton board. We changed the firmware of the cyton in order to start the data acquisition as soon as a pin, thanks to the push button, switched to a high logical level. In the same time the hc-06 bluetooth module sent an input to Smart Glasses, which began to display the sequence of images (Figure 2.7a).
   Despite this change, the problem was still present.

2. As a second step, we supposed that the delay was caused by hc-06 bluetooth module: for this reason we removed it. The starting point of the stimulation system was now the android app of Smart Glasses: We changed android apk adding an impulse sound at the beginning of the sequence of images, which went in output to the jack audio and, through an amplifier circuit, went to a cyton pin that switched to a high logical level and started the acquisition system (Figure 2.7b). The amplifier circuit was necessary because the voltage audio amplitude was smaller than 200mV.
   Even after this improvement, the epochs continued to have a random delay and consequently the processed signal continued to be wrong.

3. As a third step we found out that there was something wrong with the sampling of the USB socket. The sampling was set by default to 16 ms but the cyton sampling was set by 4 ms. We changed the first one and we verified through a NIDAQ USB-6259 that the acquisition system worked correctly (Figure 2.7c).

4. In step four, as the total system was not working properly yet, we changed the android apk adding an impulse sound every time the image display changed and the output went to a cyton channel instead of the pin, in order to verify that the changing of the images was really every 500 ms. Through both a photodiode and a little MATLAB® algorithm we saw that there was a casual delay in every image changing, caused by the slowness computing work of the java language (Figure 2.8). We modified again the android algorithm replacing the sequence of images with a pre-created video in which there was the sequence of images and an impulse sound at the beginning (Figure 2.7d).
   After this step the whole system worked rightly.

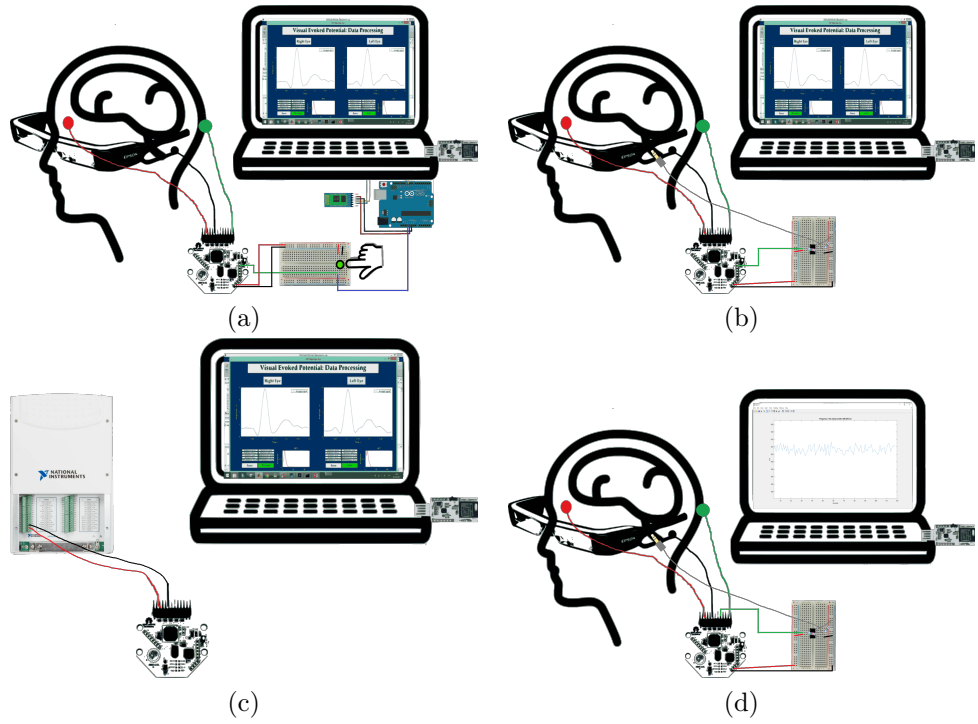

Figure 2.7: *These figure represent: (a) step one, (b) step two, (c) step three and (d) step four of the work for improving the total system and to remove the problems it presented previously.*

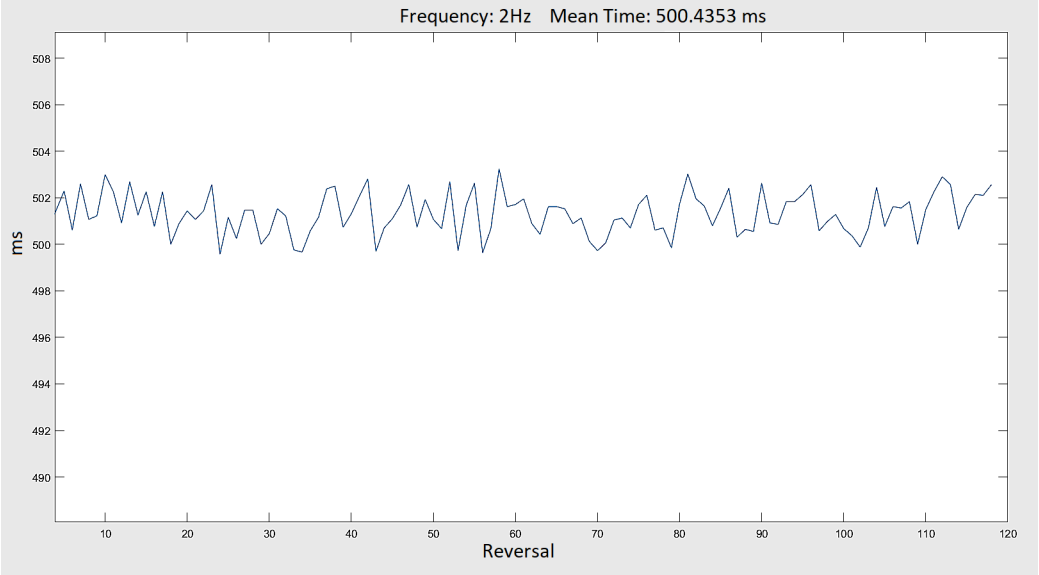

Figure 2.8: *A graph that shows the casual delay everytime the image changed.*

As a result, at present we start the stimulation system directly through the android app; as soon as the Smart Glasses displays the video, an impulse sound goes in output to the jack audio and, through an amplifier circuit, goes to a cyton pin that switches to a high logical level and starts the acquisition system. The MATLAB® algorithm displays on the pc the real time average between all the free-artifact epochs. The user can change both the temporal and the space frequency of the video: in fact, there is a database with 20 combinations.

2.6 Comfortable Improvements and CAD model

In order to refine the comfort, the following secondary improvements have been introduced:

a. The breadboard has been replaced by a prototype board, less bulky than the first one, on which the various components have been welded (operational amplifier LT1635, resistances from 2.2 and 22 kΩ, various connectors) which constitute the amplification circuit of the audio signal (Figure 2.9).

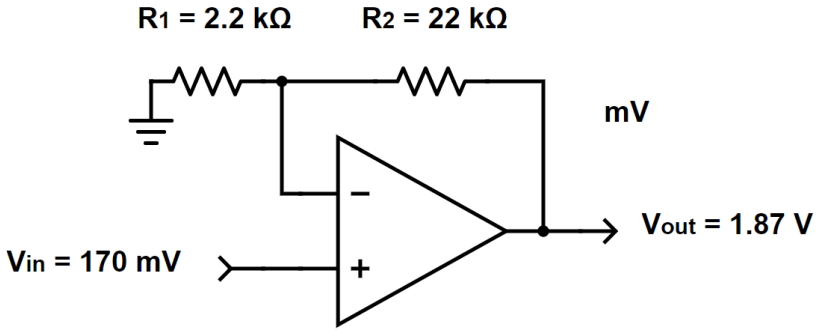

Figure 2.9: *Electric diagram of the amplification circuit*

b. The power supply, initially consisting of four 1.5V AA batteries each (Figure 2.10a), has been replaced by two CR2 batteries of 3V each one, smaller and lighter, to further reduce the overall dimensions (Figure 2.10b).

(a) (b)

Figure 2.10: *(a) Old and (b) actual cyton supply.*

Following these two modifications, a CAD model was created on Solid Works in order to contain all the components of the acquisition system (Cyton board, amplification circuit, batteries). The model, made with a 3D printer, consists of:

- A box, in which the cyton board, the two CR2 batteries and the amplification circuit are inserted inside; the box has two slits on the bottom, with an elastic band passing through, which is tightened around the patient's arm, allowing the positioning of the houses near the head of the patient (Figure 2.11a and Figure 2.11b). This is used to limit the length of the conducting cables of the electrodes, which could generate interference with the signal taken.
- A cover made with different air vents in order to dissipate the heat generated by lithium batteries (Figure 2.11c).

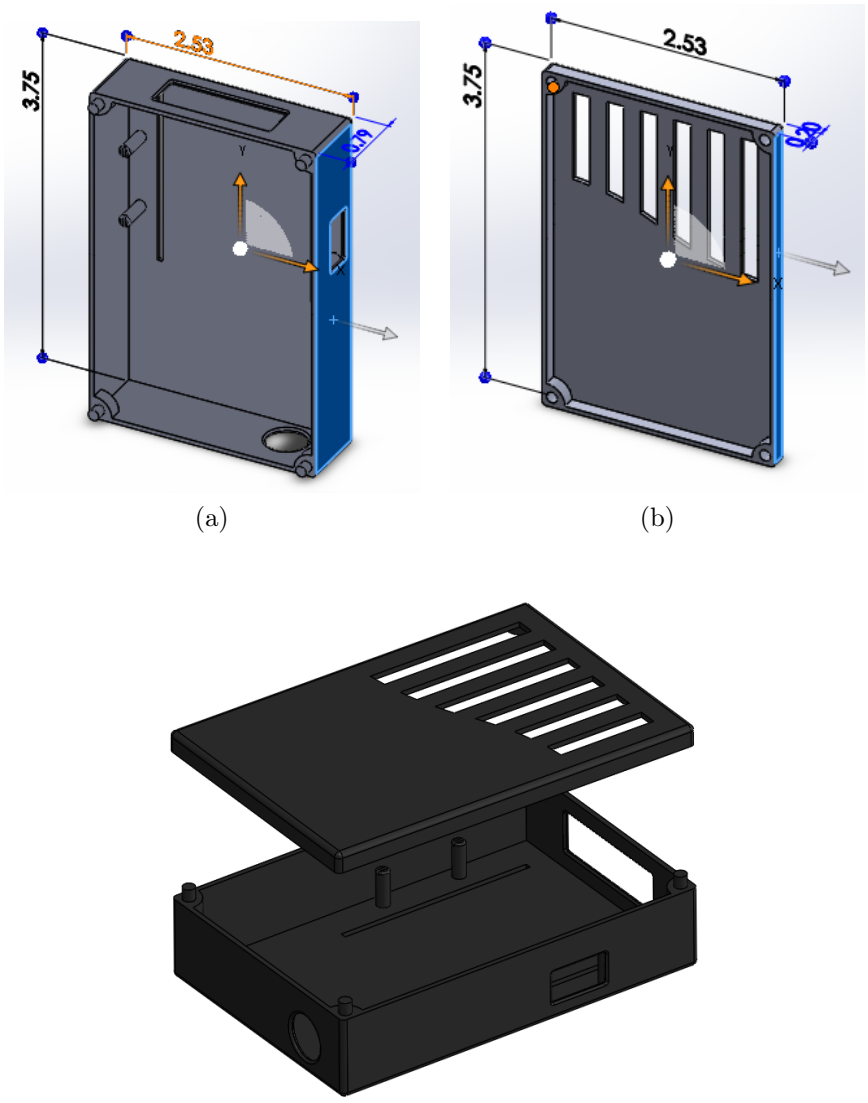

(a) (b)

(c)

Figure 2.11: *(a) Isometric view of the box, (b) isometric view of the cover and (c) complete CAD model. The dimensioning of the two pieces is expressed in cm.*

2.7 Acquisition Protocol for the Clinical Tests

In order to be able to compare our device with the Retimax, it is important to establish a precise procedure for collecting the VEP signal, making sure that it is followed in both tests. The iter to follow is illustrated in Figure 2.12:

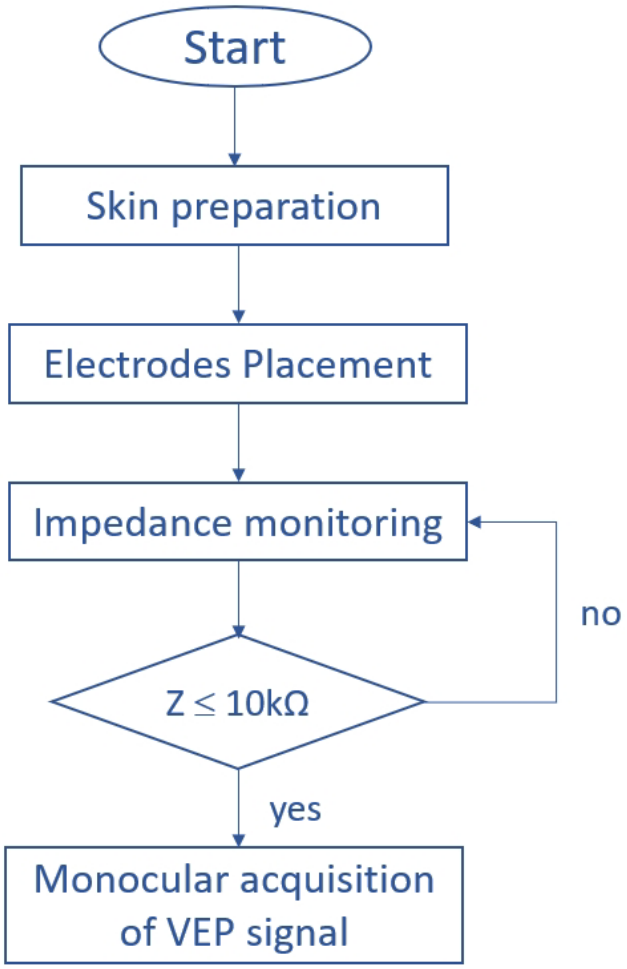

Figure 2.12: *Acquisition protocol to follow using both the Retimax CSO and our device.*

The first phase consists of patient preparation: we use a scrubbing gel (NUPREP SKIN GEL) to clean the skin portion where the electrodes will be placed is cleaned by the subject in question; in this way the dead cells are

eliminated and the electrode-skin impedance is reduced.
Afterwards, the electrodes are positioned according to the International 10/20 System, following the ISCEV standards, which are related to the repere's points and in proportion to the size of the head [31] (Figure 2.13). In our case we use three electrodes: one positioned at the point Fpz which acts as a reference, one at the point Oz which constitutes the actual sampling channel, and finally the last electrode positioned at point A2, or on the right mastoid bone, which acts as a ground.

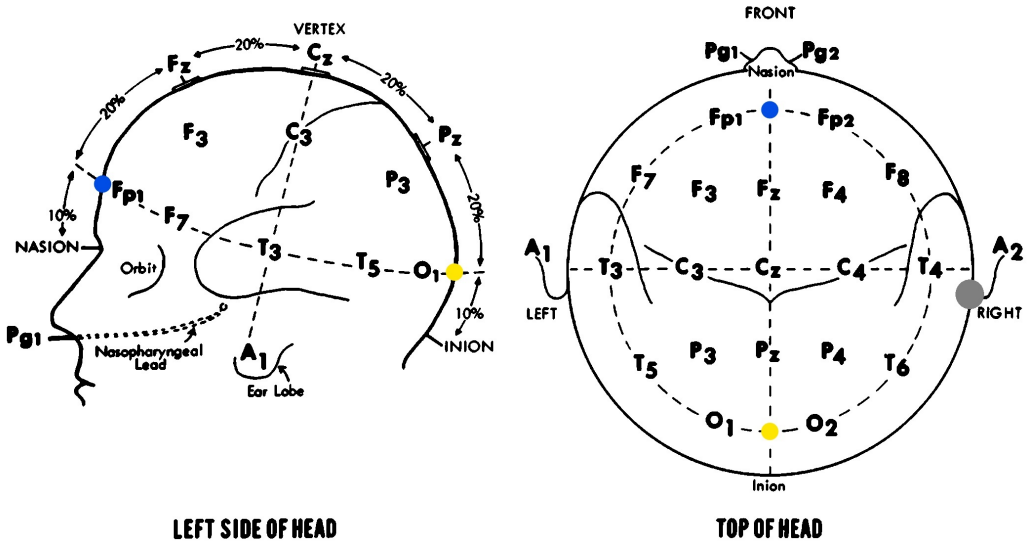

Figure 2.13: *Electrodes position made following the International 10/20 system.*

The next step involves measuring the impedance of the electrodes: to start the test, it must be smaller or equal to 10 kΩ.
Once the preparation phase has been completed, the proper clinical test begins: at the end of a 10-minute dark adaptation, an eye of the patient is covered with a blindfold and the Smart Glasses are worn (in the case of Retimax CSO, he is asked to gaze at the screen in front of him), after that the video is displayed on the respective screens and the acquisition begins.

In the center of the board there is a red dot: the subject has to fix his eye on it for the duration of the exam. The test has a duration of 60 seconds, needed to acquire 120 epochs of 500 ms each, which are processed removing

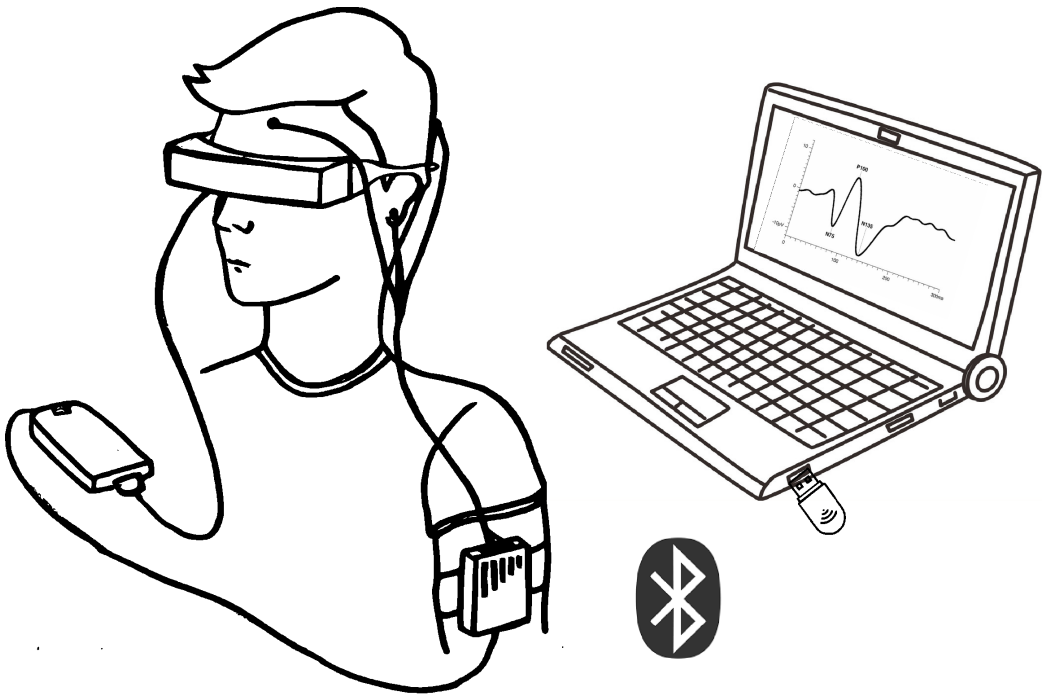

Figure 2.14: *A representation of our device while it is working.*

the artifacts such as blinking artifacts or motion artifacts: the average value is first removed from the signal; after that, it is filtered with a band-pass filter at 1-30 Hz and finally all epochs with one or more values higher than 50 μV are removed, as containing blinking artifacts.
During the acquisition of the various epochs, the average of the selected periods is gradually accomplished and displayed on the PC screen.
An important factor to take into consideration is the initial trigger of the acquired signal: in fact, the image display has an expected delay as to the initial input that the PC sends, which induces a translation of the waves of the VEP to the left. After various experiments we deduced that the delay was exactly equal to 76 ms. By eliminating the first epoch, which could be corrupted by error, the average algorithm starts from sample 106 (considering that the acquisition board has a sampling frequency of 250 Hz, each sample corresponds to 4 ms and therefore the algorithm analyzes data that were acquired after 424 ms).

As to the Retimax CSO, the exam does not have a fixed duration, but ends when 100 free artifact epochs are reached; this may imply a longer duration of the test.
The same procedure is performed with the other eye.

Both instruments used must characterize the stimulation pattern with the parameters described in Table 2.1.

Table 2.1: *Standard values of the parameters to be selected*

Parameter	**Selected value**
Temporal Frequency (Hz)	2
Spatial Frequency (MoA)	60
Aspect Ratio	16:9
Contrast (%)	81

As already mentioned in paragraph 2.6, the first two parameters (temporal frequency and spatial frequency) can be modified according to a database with a selection of 20 different combinations:

1. Four different temporal frequency (2, 4, 5, 6 Hz);
2. Five different space frequency (15, 30, 60, 120, 240 MoA).

We used what we consider the standard values for this type of examination.

As to the first parameters, using a lower frequency implies:

- Less fatigue of the patient's eye and therefore the possibility of carrying out the same test several times;
- A very low probability of inducing epileptic crisis.

The choice to set the contrast to 81% has been dictated by LCD screen of smart glasses. An important difference between LCD screen of Smart Glasses and CRT display of Retimax CSO involves how the screen pixels emit light: the CRT display generates a light emitting that lasts about 2 ms when a frame appears, while an LCD screen maintains a constant luminance for a shorter time for each frame. The luminance curve of an LCD screen therefore has an asymmetrical profile, called "rising and falling" and this generates a change in luminance, which leads to an artifact of luminance whenever the checkerboard inverts the pattern.
Moreover, an LCD stimulator must generate stimuli that are not significantly small and do not cause interference. The luminance stability is also influenced by the temperature of the environment and the angle of vision.

The previous part of the study had shown that in multifocal VEPs on healthy subjects the luminance artifact can be reduced by reducing the contrast of the pattern. After some experiments, in study [1] it was confirmed that the ideal contrast to reduce the artifact is 81%.

Chapter 3

Statistic Analysis

In order to verify the accuracy of the results obtained with the new device, a statistic analysis was made comparing the signals obtained from the tests performed with the Smart Glasses, with the signals obtained by performing the tests with the Retimax Advanced CSO.
The statistic analysis of the acquired data that was decided to use was based on the morphology of the VEP signal; in particular, 10 precise characteristics were analyzed (Figure 3.1):

- **N75 Amplitude**;
- **P100 Amplitude**;
- **N135 Amplitude**;
- **N75 Latency or Time To Peak (TTP)**;
- **P100 TTP**;
- **N135 TTP**;
- **N75-P100 Amplitude**;
- **P100-N135 Amplitude**;
- **N75-P100 TTP**;
- **P100-N135 TTP**.

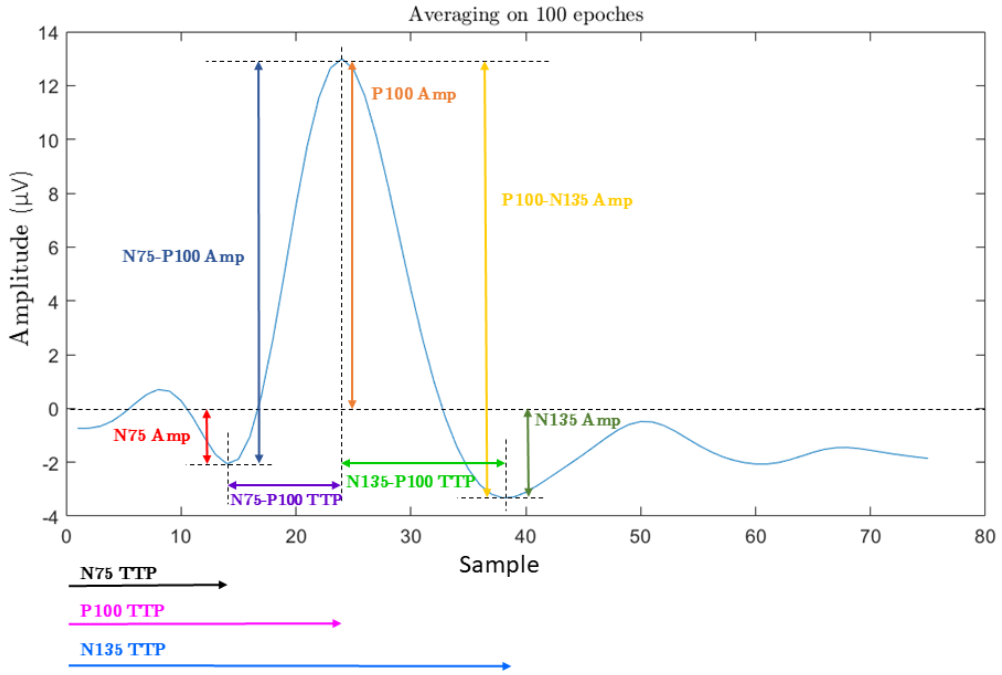

Figure 3.1: *The ten features that were analyzed in our work.*

These characteristics have been inserted into some statistical analysis algorithms:

1. **Kolmogorov-Smirnov test**: is a NON parametric test used by us only to evaluate the normality of the data. In fact, if the data did not have a Gaussian distribution and therefore did not respect the condition of normality, the paired t test would not be performed, as the obtained p-values would not be statistically reliable. This test calculates the distance between a function $\hat{F}_n(x)$ considered true (in our case the values obtained through the Retimax CSO) and an empirical function $F_0(x)$ (in our case the values obtained through the Smart Glasses). The following is used as distance:

$$D_n = \sup_{-\infty<x<+\infty} |\hat{F}_n(x) - F_0(x)|$$

We take into consideration the greatest: if this exceeds a predetermined value, the hypothesis of normality is rejected. Otherwise it is not rejected. [32]

2. **Paired t-test**: is a parametric test that checks if the mean value of a given distribution differs significantly from a certain reference value. It can be used, as in our case, to compare two measurement methods applied to the same subject.
   The difference between the two measures is calculated and averaged ($\overline{d} = \overline{y - x}$); then the standard deviation is calculated and from that the standard error of the mean difference is derived ($SE(\overline{d}) = \frac{s_d}{\sqrt{n}}$). It is then calculated the t-statistic ($T = \frac{\overline{d}}{SE(\overline{d})}$) and finally the tables of the t-distribution is used to compare the value for T to the t_{n-1} distribution. This will give the p-value for the paired t-test. Smaller values of the p-value indicate a greater correlation between the two datasets; the upper limit of p-value was set at 0.05 [33].

3. **Bland-Altman Plot**: is a method of data analysis aimed at verifying the comparability between two measurement techniques of the same nature. More precisely, this is a scatter plot, where the arithmetic mean of the two measurements (reference values) is shown on the abscissae and the difference between the two measurements is shown on the ordinates. The horizontal line in the middle represents the average of the differences: values above or below indicate an overestimation or underestimation of one method with respect to the other. The other two horizontal lines represent the mean of the differences ± 1.96 * SD, limiting the confidence interval within these: if the points of the graph are within this range the two methods can be considered congruent [34].

4. **Scatter-plot**: is a type of graph in which two variables of a data set are shown on a Cartesian plane.
   A scatter plot is often used when one of the variables is under the control of the experimenter. A parameter that is incremented and / or systematically decremented is called an independent or variable control parameter, and it is arbitrarily placed on the horizontal axis. The measured variable (or dependent) is arbitrarily placed on the vertical axis. Scatter plot can be useful to visualize the correlation degree

between the two variables (that is linear dependence). [35]

After that, a table has been displayed containing average and standard deviation of the values obtained through the retimax and the same has been done for those of Smart Glasses. Moreover, the difference between the means of the values obtained through the two devices has been visualized. This procedure was done by separating the results of the left eye and right eye. Finally, a purely visual morphological comparison was made by projecting the traces of the tests performed on the two instruments onto a single chart, overlapping them.

Chapter 4

Results

4.1 Recalibration with Healthy Subjects

For the recalibration of the device, 10 healthy subjects were recruited, of which 7 males and 3 females, with an age of 25.14 ± 1.46 years (see Table 4.1), for a total of 20 eyes. Each subject was selected taking into account that no one had a history of ophthalmological diseases and visual acuity was measured: all the subjects were considered healthy and they was opportunely refracted with glasses in case of necessity. Furthermore, all the patients were previously informed about the test they were going to do and gave their consent.

Table 4.1: *Clinical details of the subjects recruited: subject, gender, age and visual correction for left (L) and right (R) eye.*

Subject	Gender	Age	Visual correction (L)	Visual correction (R)
AM	Male	24.3	None	None
GA	Male	25.7	Contact lens (0.50 D)	Contact lens (0.25 D)
GDL	Male	24.3	None	None
MC	Male	24.6	Contact lens (0.75 D)	Contact lens (0.25 D)
MCS	Male	25.9	None	None
RT	Female	24.3	Contact lens (2.75 D)	Contact lens (2.75 D)
SC	Female	24.9	None	None
FR	Male	25.4	None	None
DC	Female	26.6	Contact lens (2.00 D)	Contact lens (2.50 D)
CP	Male	25.4	None	None

As illustrated in the previous chapter, the data obtained were elaborated so as to extrapolate the ten most characteristic features; subsequently, all of the analysis described were carried out.
First, the Kolmogorov-Smirnov test was performed to verify the normality of the data (Table 4.2).

Table 4.2: *This table shows the maximum distance obtained from the Kolmogorov-Smirnov test performed on the 10 features of the healthy subjects and the outcome of normality, for both eyes. "R" in case of normality rejected, "A" in case of normality accepted.*

	Left Eye		Right Eye	
	D_{max}	Normality	D_{max}	Normality
Amplitude (μV)				
N75 Amplitude	0.5581	R	0.5138	R
P100 Amplitude	0.5954	R	0.4492	R
N135 Amplitude	0.4169	R	0.6808	R
N75-P100 Amplitude	0.7772	R	0.5553	R
P100-N135 Amplitude	0.6978	R	0.7223	R
Latency (ms)				
N75 Amplitude	0.6000	R	0.7000	R
P100 Time Peak	0.6000	R	0.4000	R
N135 Time Peak	0.9000	R	0.6000	R
N75-P100 Amplitude	0.7000	R	0.8000	R
P100-N135 Amplitude	0.7000	R	0.7000	R

From the table emerges rejection of normality for all 10 features due to the fact that, being a preliminary analysis, the amount of data analyzed is not sufficient to create a Gaussian distribution. Therefore, based on these results, the parametric t-test could not be performed.

Then, for each feature, a scatter plot and a bland-altman plot were made (Figure 4.1). In addition to the plots, some features have been shown.

Particularly, for the correlation plot are displayed:

- The number of data point used (n);
- The pearson r-value (r);
- The pearson r-value squared (r^2);
- The intercept equation.

Instead, for the Bland-Altman plot are displayed:

- The reproducibility coefficient (RPC), that is 1.96 * SD, with its percent value;
- The coefficient of variation (CV), that is the standard deviation of mean values in %.

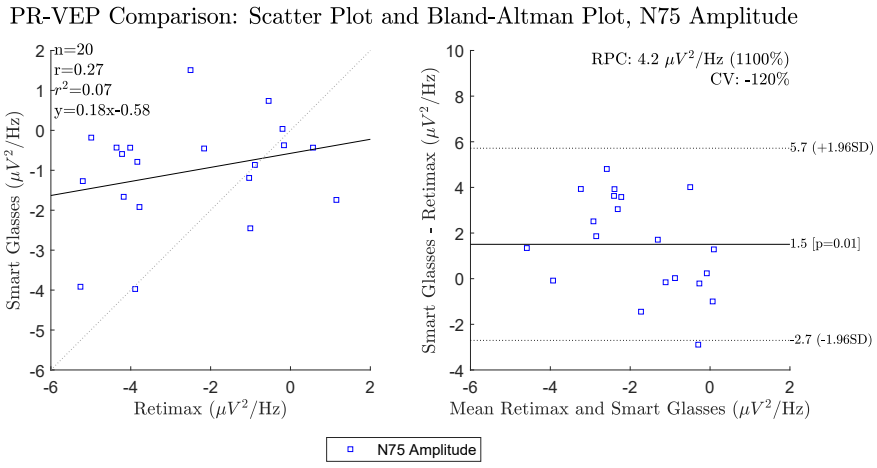

PR-VEP Comparison: Scatter Plot and Bland-Altman Plot, P100 Amplitude

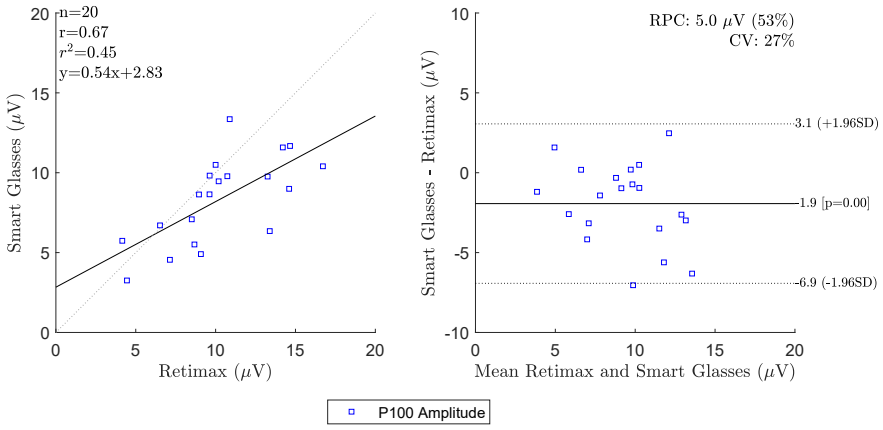

PR-VEP Comparison: Scatter Plot and Bland-Altman Plot, N135 Amplitude

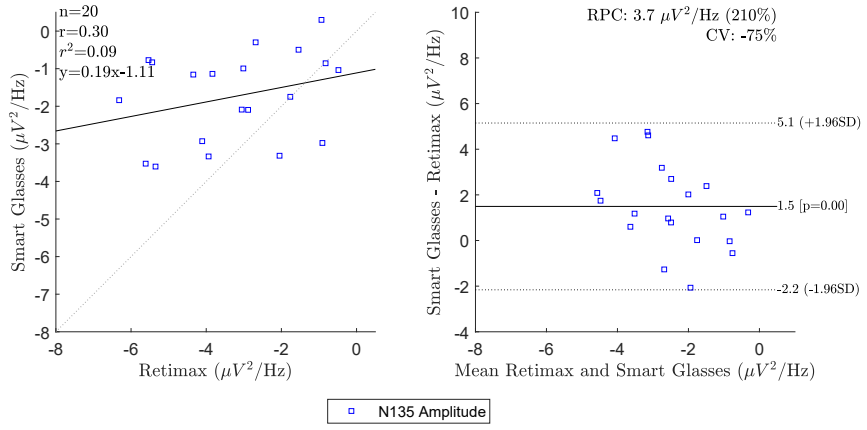

PR-VEP Comparison: Scatter Plot and Bland-Altman Plot, N75-P100 Amplitude

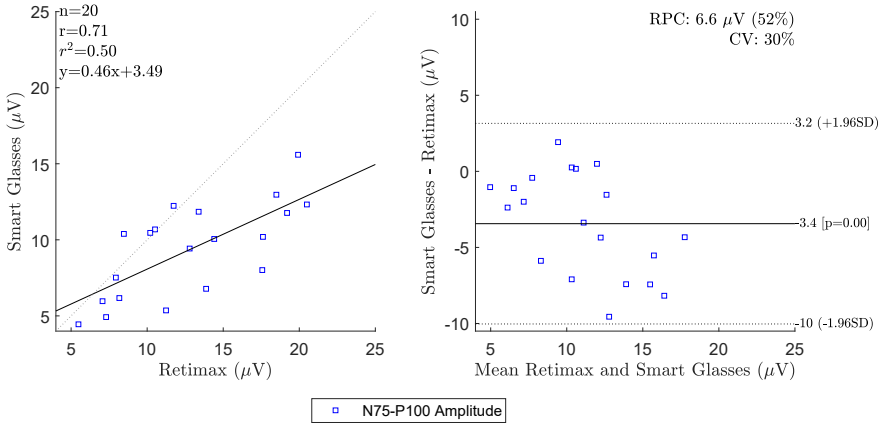

PR-VEP Comparison: Scatter Plot and Bland-Altman Plot, N135-P100 Amplitude

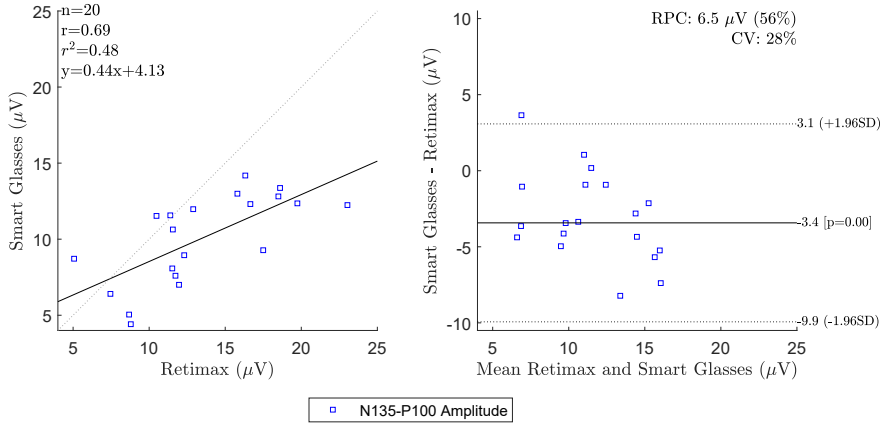

PR-VEP Comparison: Scatter Plot and Bland-Altman Plot, N75 Latency

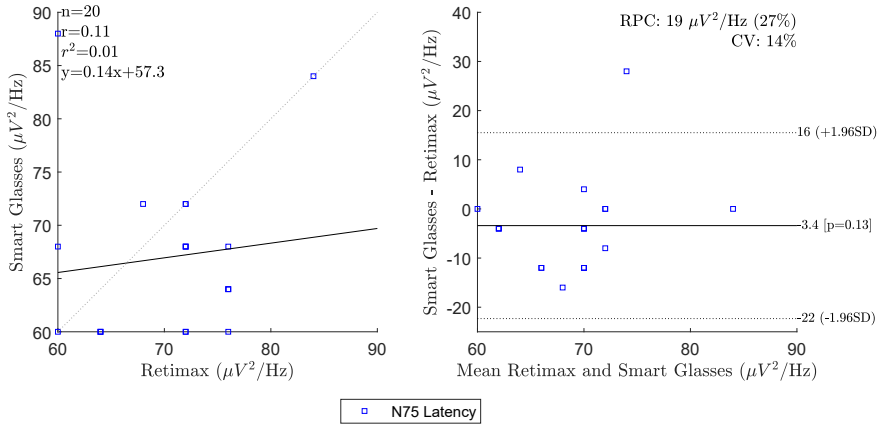

PR-VEP Comparison: Scatter Plot and Bland-Altman Plot, P100 Latency

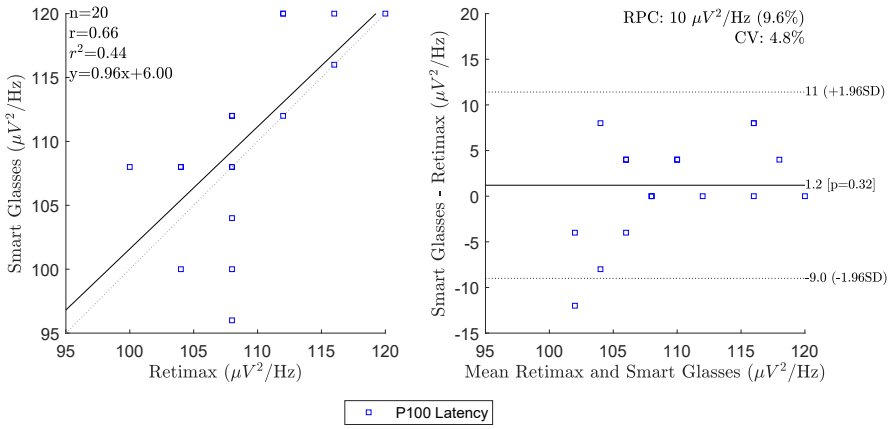

PR-VEP Comparison: Scatter Plot and Bland-Altman Plot, N135 Latency

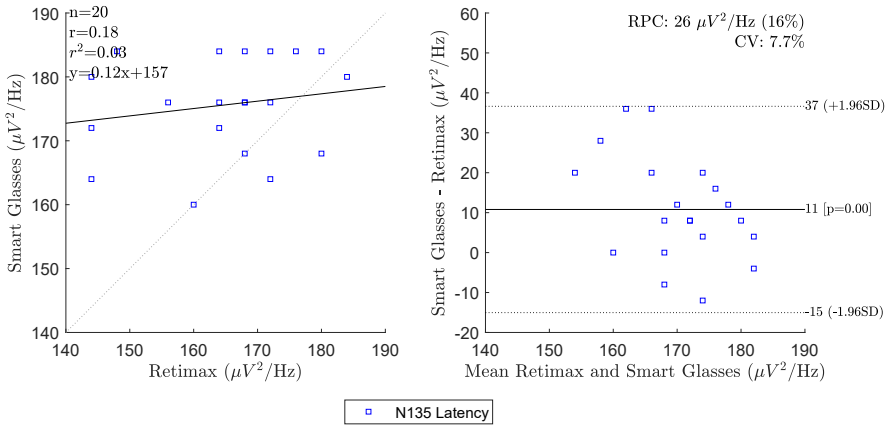

PR-VEP Comparison: Scatter Plot and Bland-Altman Plot, N75-P100 Latency

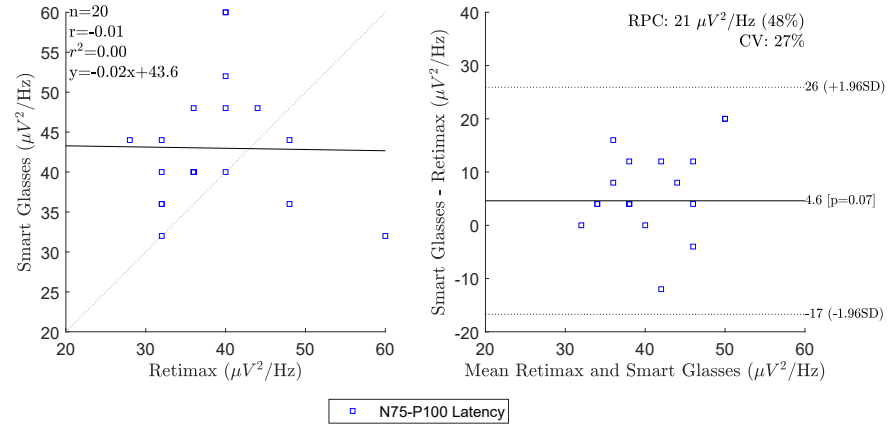

PR-VEP Comparison: Scatter Plot and Bland-Altman Plot, N135-P100 Latency

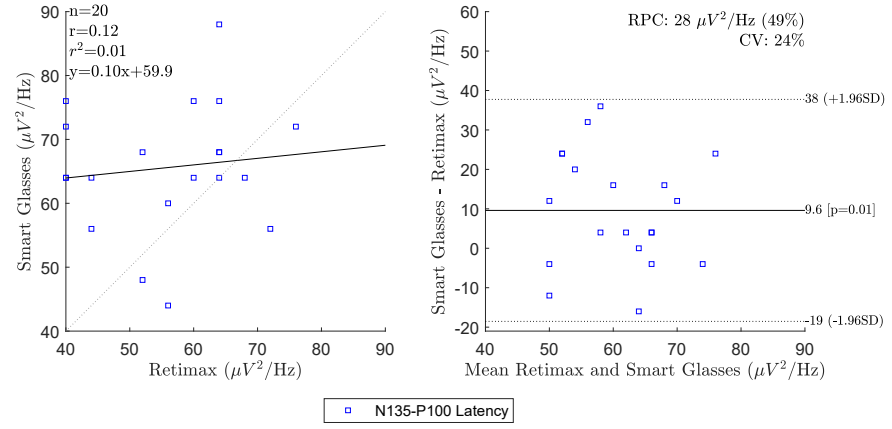

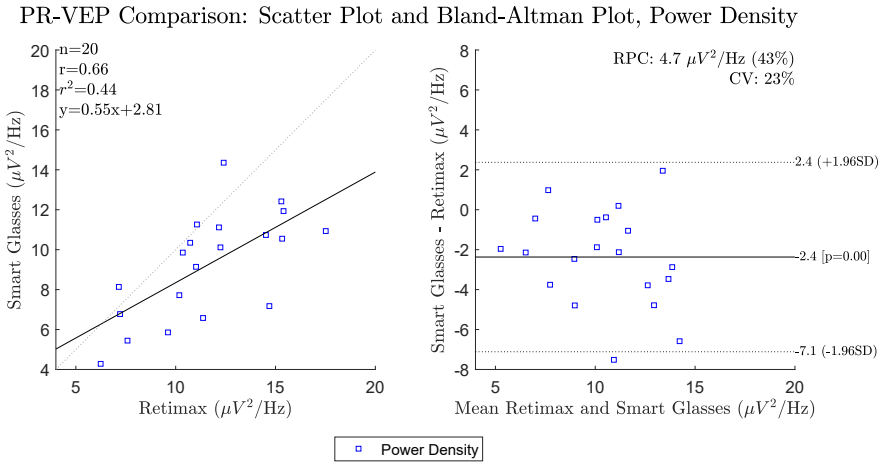

Figure 4.1: *Scatter plot and Bland-Altman plot of the ten features analyzed and of the power density for the healthy subjects.*

As far as scatter plots are concerned, the most marked similarity is certainly the latency of the p100 wave: the intercept line is placed practically on the bisector of the quadrant (slope of the line $\simeq 1$), which indicates that the two datasets are almost identical. An excellent result is obtained also for the P100 amplitude, which has a slope of the line of 0.54 and a Pearson r-value of 0.67, that represents a strong correlation between the data. Similar results are also obtained for the relative amplitudes N75-P100 and N135-P100 (respectively slope of the line = 0.46 and Pearson r-value = 0.71, slope of the line = 0.44 and Pearson r-value = 0.69).
Finally, the worst results are obtained with the relative latencies N75-P100 and N135-P100 (respectively slope of the line = -0.02 and Pearson r-value = 0.01, slope of the line = 0.10 and Pearson r-value = 0.12).

The Bland-Altman graphs were obtained to evaluate a possible systematic error by calculating the *bias* obtained as the average of all the differences and the relative 95% confidence interval.
In 60% of cases (6 graphs out of 10) there is a bias that produces an overestimation for low values and an underestimation for high values.
On the other hand, as far as the disposition of the data is concerned, in the

majority of cases all fall within the 95% confidence interval.

Then, a comparison was made between the average of the data obtained with the Retimax and that of the data obtained with the Smart Glasses, calculating the difference in absolute value and represent it also in percentage terms. Furthermore, in this case the left and right eye data have been separated to understand if there are any systematic errors in the stimulation of one of the two eyes. The results can be seen in Table 4.3 and 4.4.

Table 4.3: *Left eye: differences between Retimax and Smart glasses stimulations in terms of PR-VEP amplitudes and latencies. Values are presented as mean ± standard deviation. In the last row is also presented the power density of PR-VEP derived from both instruments. In the last column the absolute means difference are shown (AMD) and the relative decrease percentage.*

	Left Eye		
	Retimax	Smart Glasses	AMD
Amplitude (μV)			
N75 Amplitude	-2.89 ± 1.85	-1.18 ± 1.25	1.71 (59%)
P100 Amplitude	10.45 ± 3.65	7.95 ± 2.45	2.50 (23%)
N135 Amplitude	-2.90 ± 2.15	-2.18 ± 1.14	0.72 (24%)
N75-P100 Amplitude	13.35 ± 4.44	9.14 ± 3.06	4.21 (31%)
P100-N135 Amplitude	13.35 ± 5.21	10.14 ± 2.87	3.21 (24%)
Latency (ms)			
N75 Time To Peak	70.8 ± 7.06	67.2 ± 7.49	3.6 (5%)
P100 Time To Peak	108 ± 4.61	110.4 ± 7.10	2.4 (2%)
N135 Time To Peak	164 ± 12.07	176.4 ± 8.73	12.4 (7%)
N75-P100 Time To Peak	37.2 ± 5.97	43.2 ± 7.72	6.00 (13%)
P100-N135 Time To Peak	56 ± 9.97	66 ± 8.27	10 (15%)
Frequency Domain ($\mu V^2/Hz$)			
Power Density	11.86 ± 3.28	8.93 ± 2.43	2.93 (24%)

From Table 4.3 emerge the following information: all the amplitude of the Smart Glasses are smaller than those of the Retimax; most of the values undergo an average decrease of about 25%. The greatest decrease is observed in the amplitude of the N75 wave, which has a value that has more than halved (59%).

As regards instead the latencies, the results obtained are practically the same for the two instruments: the means show an increase of 2% for the latencies of the P100 wave, a decrease of 5% for the N75 wave and a raise of 7% for the N135 wave. The values of the relative latencies N75-P100 and N135-P100 differ slightly, even if the results are still excellent: in this case the

Smart Glasses increase the latencies measured by the Retimax by a value of respectively 13% and 15%. Finally, the power density shows a decrease in the case of smart glasses of 24%.

Table 4.4: *Right eye: differences between Retimax and Smart glasses stimulations in terms of PR-VEP amplitudes and latencies. Values are presented as mean ± standard deviation. In the last row is also presented the power density of PR-VEP derived from both instruments. In the last column the absolute means difference are shown (AMD).*

	Right Eye		
	Retimax	Smart Glasses	AMD
Amplitude (μV)			
N75 Amplitude	-2.15 ± 2.32	-0.85 ± 1.47	1.30 (60%)
P100 Amplitude	10.08 ± 3.30	8.71 ± 3.01	1.37 (13%)
N135 Amplitude	-3.55 ± 1.48	-1.29 ± 1.11	2.26 (63%)
N75-P100 Amplitude	12.23 ± 5.22	9.56 ± 3.23	2.67 (21%)
P100-N135 Amplitude	13.64 ± 4.17	10.00 ± 3.10	3.64 (26%)
Latency (ms)			
N75 Time To Peak	70 ± 6.32	66.8 ± 8.65	3.20 (4%)
P100 Time To Peak	109.6 ± 5.05	109.6 ± 7.10	0.00 (0%)
N135 Time To Peak	165.6 ± 12.95	174.8 ± 6.81	9.20 (5%)
N75-P100 Time To Peak	39.6 ± 8.73	42.8 ± 8.44	3.20 (8%)
P100-N135 Time To Peak	56 ± 13.33	65.2 ± 12.08	9.20 (16%)
Frequency Domain ($\mu V^2/Hz$)			
Power Density	11.34 ± 3.17	9.53 ± 2.91	1.82 (16%)

As regards the right eye we can extract information similar to those of the left one. Among the amplitudes the best result is obtained with the wave P100, which undergoes a decrease of 13% in the case of Smart Glasses. Good results are also obtained with the relative amplitudes N75-P100 and N135-P100, which decrease by a value of 21% and 26%, respectively. Finally, the amplitudes N75 and N135 have more than halved (they have a decrease

of 60% and 63% respectively).
For what concern the latencies, the results are excellent and very similar to those obtained with the other eye. N75 Time To Peak suffers a slight decrease (4%), N135 Time To Peak has a higher value than the Retimax of 5%, while the latency of the P100 wave is exactly the same. The relative latencies N75-P100 and N135-P100 undergo an increase of the values equal to respectively 8% and 16%. Finally, the value of the power density decrease of 16% in the case of the Smart Glasses.

The last statistical analysis is the strictly visual one. For each test performed a morphological comparison was made, going overlapping the tracks obtained with the Retimax and Smart Glasses. The best VEPs, for both eyes, of all the patients, is presented below.

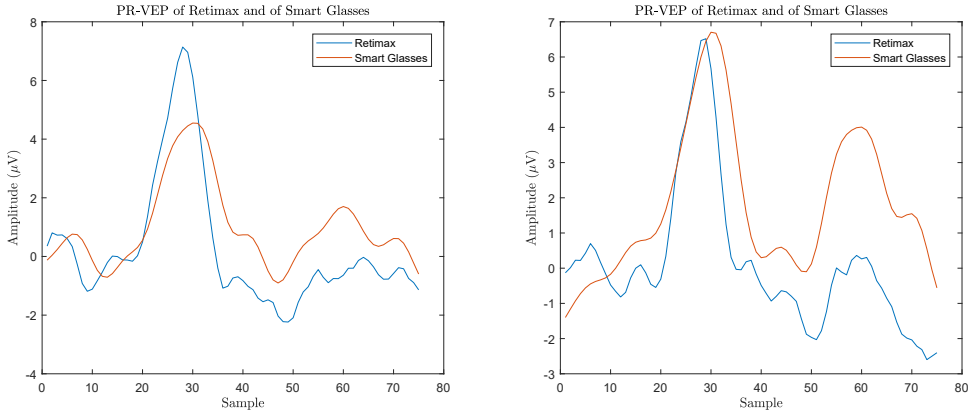

Figure 4.2: *Patient A.M.: on the left, the tracks of the left eye; on the right, the tracks of the right eye.*

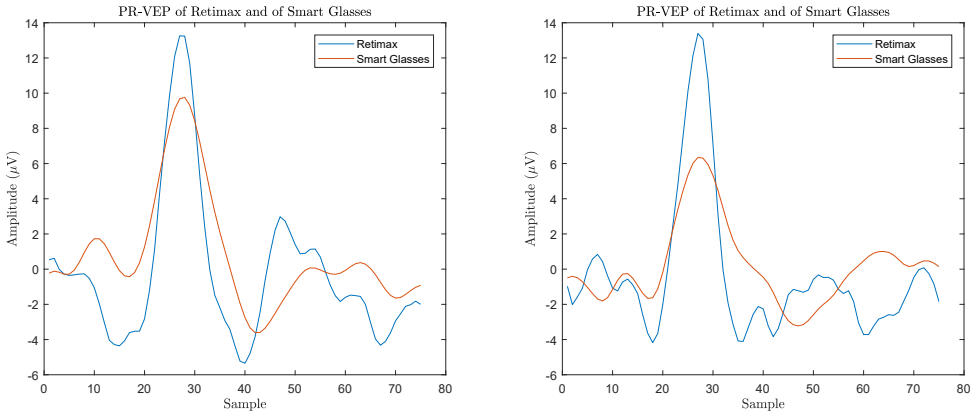

Figure 4.3: *Patient G.A.: on the left, the tracks of the left eye; on the right, the tracks of the right eye.*

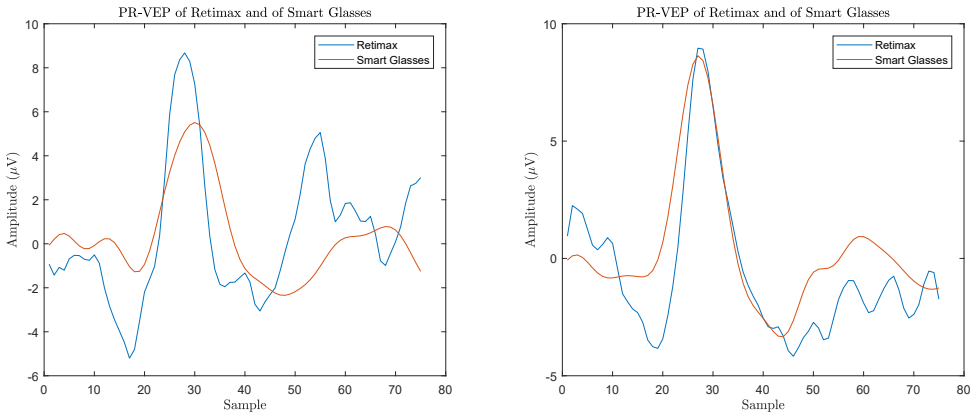

Figure 4.4: *Patient G.D.L.: on the left, the tracks of the left eye; on the right, the tracks of the right eye.*

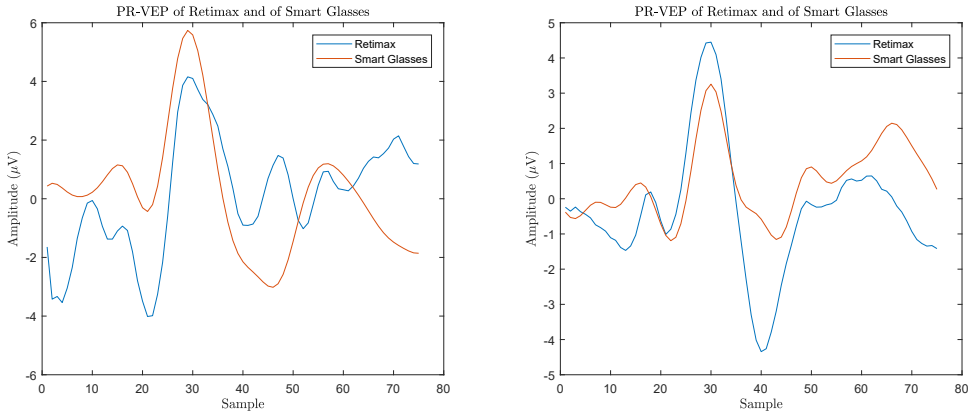

Figure 4.5: *Patient M.C.: on the left, the tracks of the left eye; on the right, the tracks of the right eye.*

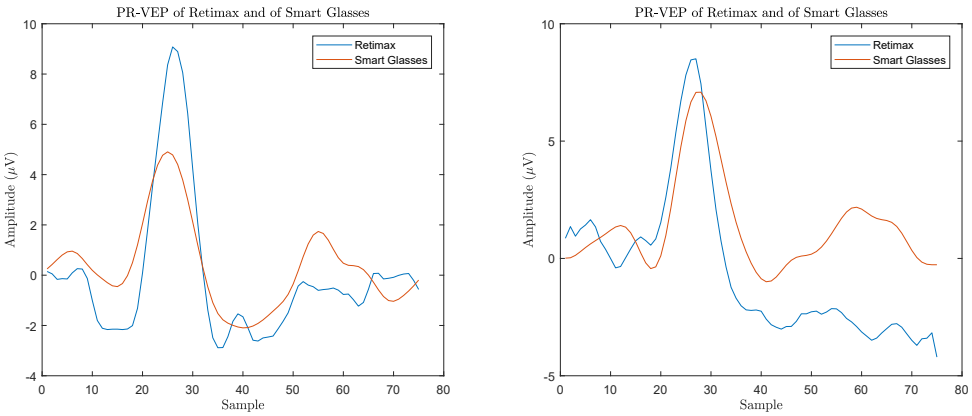

Figure 4.6: *Patient M.C.S..: on the left, the tracks of the left eye; on the right, the tracks of the right eye.*

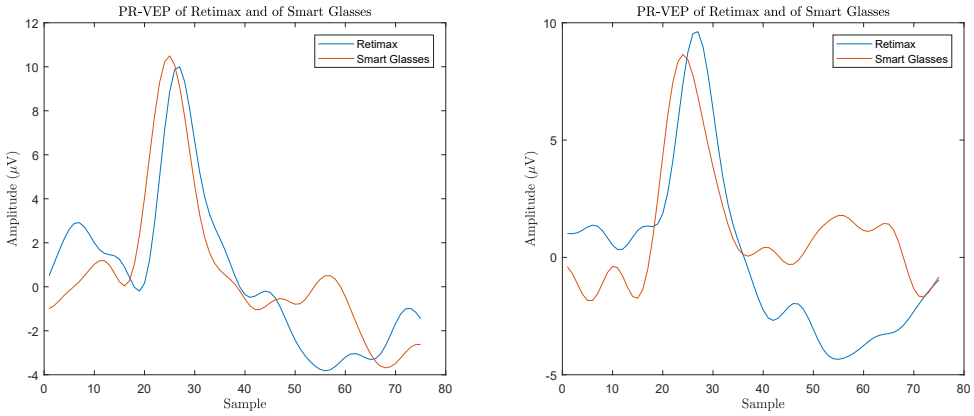

Figure 4.7: *Patient R.T.: on the left, the tracks of the left eye; on the right, the tracks of the right eye.*

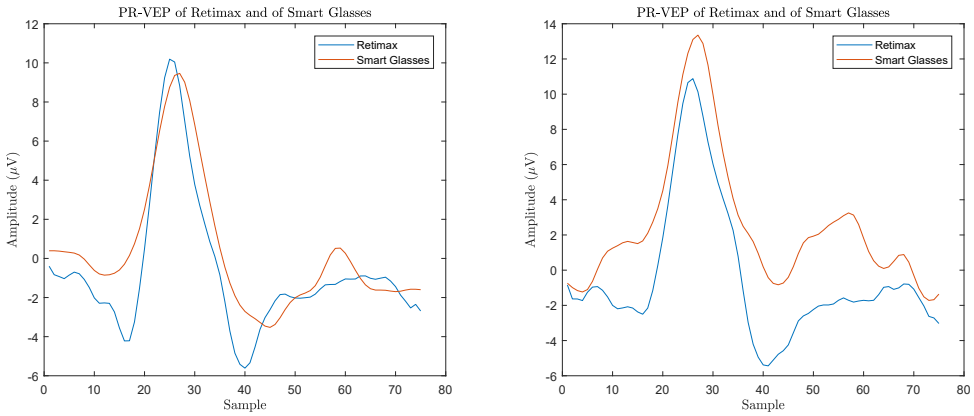

Figure 4.8: *Patient S.C.: on the left, the tracks of the left eye; on the right, the tracks of the right eye.*

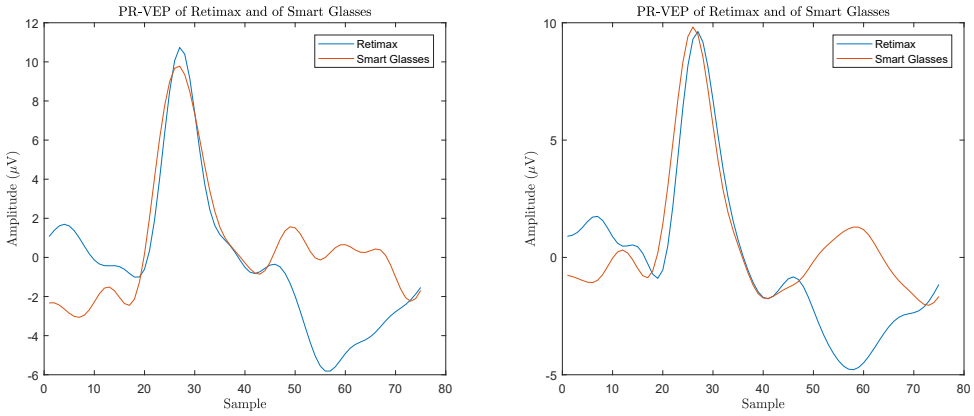

Figure 4.9: *Patient F.R.: on the left, the tracks of the left eye; on the right, the tracks of the right eye.*

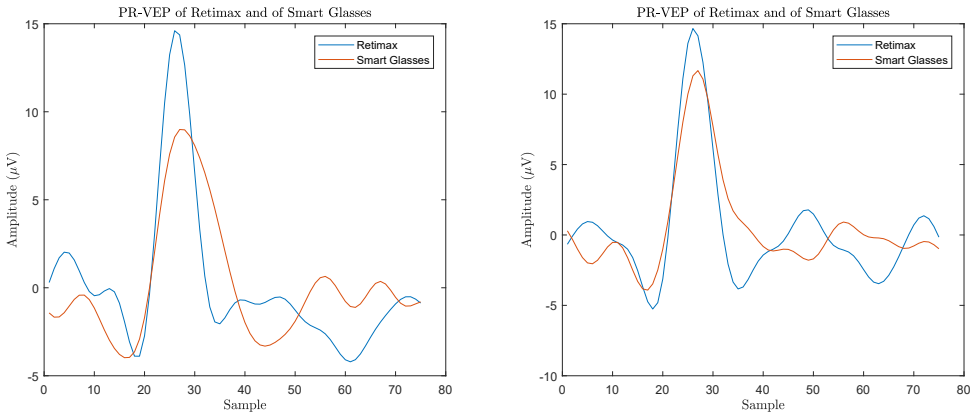

Figure 4.10: *Patient D.C.: on the left, the tracks of the left eye; on the right, the tracks of the right eye.*

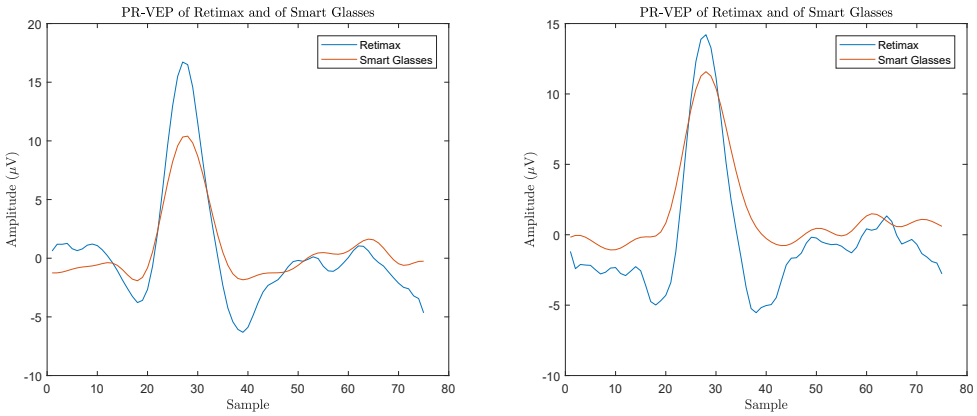

Figure 4.11: *Patient C.P.: on the left, the tracks of the left eye; on the right, the tracks of the right eye.*

Looking at the above graphs, it is possible to see the same trend previously analyzed for almost all the tracks.
In 14 cases out of 20, the amplitude of the P100 wave (the most important as well as the most evident) has a smaller amplitude in the case of Smart Glasses, while its latency is almost identical in the two cases. Moreover, the two negative waves are less pronounced than the Retimax in 13 cases out of 20.

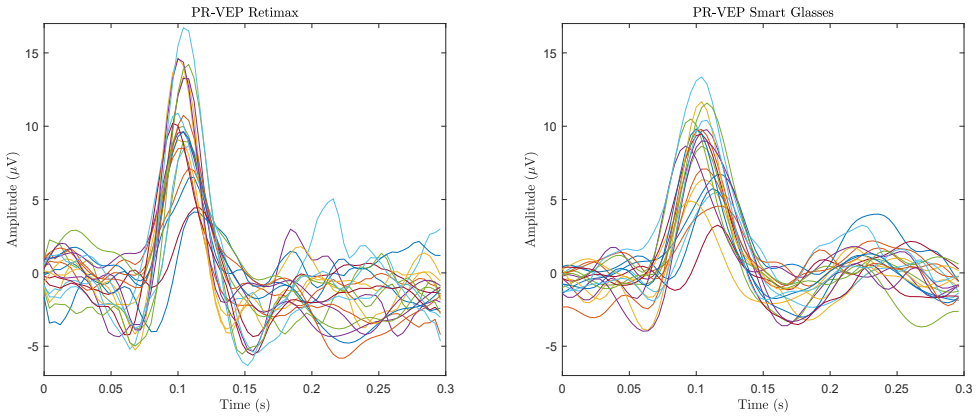

Figure 4.12: *All the PR-VEP waveforms obtained during the test, using the Retimax stimulator (a) and the smart glasses (b). The PR-VEPs obtained showed very similar potentials, well-defined in terms of N75, P100, and N135 components.*

4.2 Acquisitions on Pathologic subjects

After a satisfying recalibration, it proceeded to perform a clinical trial on pathologic subjects to verify that the device worked correctly even in the case of more complicated signals.
For this trial, 11 pathologic subjects were recruited, of which 3 males and 8 females, with an age of 67.27±12.73 years (see Table 4.5), for a total of 22 eyes. All the patients were previously informed about the test they were going to do and gave their consent.
Everyone has an eye condition that is part of the same large family of *maculopathies*. Maculopathy, or *macular degeneration*, is a disease that involves the central part of the retina known as the macula. It is characterized by the progressive loss of central vision that strongly limits the visual function. The most frequent type of maculopathy is senile [36]; other types of maculopathy identified in this study are:

- *Myopic maculopathy*: as in a myopic eye the eyeball is not spherical but instead is too long, the walls of the eyeball become extremely stretched and thin. The layers at the back of the eye can become so thin that cells

in the retina begin to die. This leads to a slow decline in central vision. Symptoms include distorted images and blurred or missing spots in the vision [37];

- *Diabetic maculopathy*: there is an accumulation of extracellular fluid in the inner nuclear layer of the retina. Symptoms include a blurring of central vision [38].

- *Exudative maculopathy after retinal venous thrombosis*: it is the presence of hemorrhages and fluid exudation within the macula due to an occlusion tipically located at an arterio-venous crossing site. symptoms include the gradually visual loss [39];

- *Choroidal Neo-Vascularization (CNV)*: it leades the growth of new blood vessels that originate from the choroid through a break in the subretinal space. Symptoms are painless loss of vision [40].

Table 4.5: *Clinical details of the pathologic subjects recruited: subject, gender and age.*

Subject	Gender	Age
RE	Male	73
RN	Female	64
RA	Female	72
RG	Male	80
TG	Male	65
TE	Female	58
TGP	Female	71
TL	Female	56
VM	Female	62
VMA	Female	69
VR	Female	70

In the same way as in the previous chapter, the 10 features are extracted from the VEP signals before being inserted into the statistical algorithms

and analyzed.
First, the Kolmogorov-Smirnov test was performed to verify the normality of the data (Table 4.6).

Also in this case, the results show that the patients are not in sufficient numbers to have a Gaussian distribution of the data; as a consequence, normality is rejected in 19 cases out of 20 and the paired t-test could not be performed.

Table 4.6: *This table shows the maximum distance obtained from the Kolmogorov-Smirnov test performed on the 10 features of the pathologic subjects and the outcome of normality, for both eyes. "R" in case of normality rejected, "A" in case of normality accepted.*

	Left Eye		Right Eye	
	D_{max}	Normality	D_{max}	Normality
Amplitude (μV)				
N75 Amplitude	0.4684	R	0.3631	R
P100 Amplitude	0.3852	R	0.3655	R
N135 Amplitude	0.6374	R	0.6537	R
N75-P100 Amplitude	0.2889	R	0.2466	A
P100-N135 Amplitude	0.5658	R	0.7296	R
Latency (ms)				
N75 Amplitude	0.6364	R	0.6364	R
P100 Time Peak	0.5455	R	0.6364	R
N135 Time Peak	0.4545	R	0.7273	R
N75-P100 Amplitude	0.6364	R	0.7273	R
P100-N135 Amplitude	0.4545	R	0.7273	R

Subsequently, for each features a scatter plot and a Bland-Altman plot were made (Figure 4.13), with the aim of identifying the level of similarity between the data obtained from Smart Glasses and Retimax and to detect any bias or systematic errors.

PR-VEP Comparison: Scatter Plot and Bland-Altman Plot, N75 Amplitude

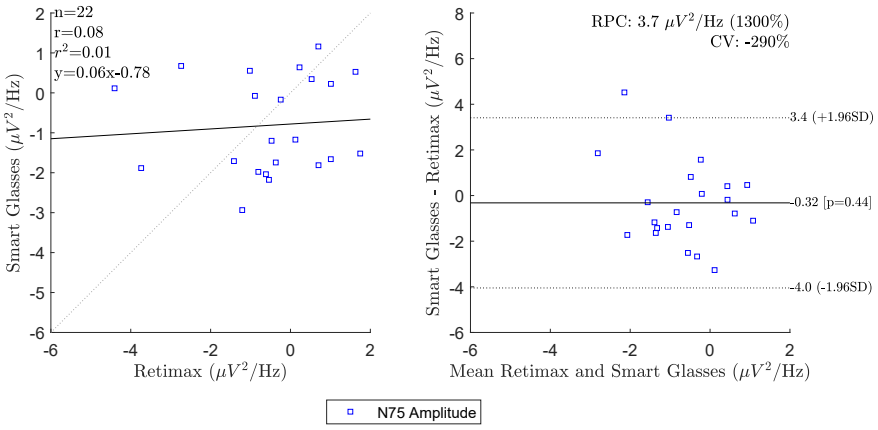

PR-VEP Comparison: Scatter Plot and Bland-Altman Plot, P100 Amplitude

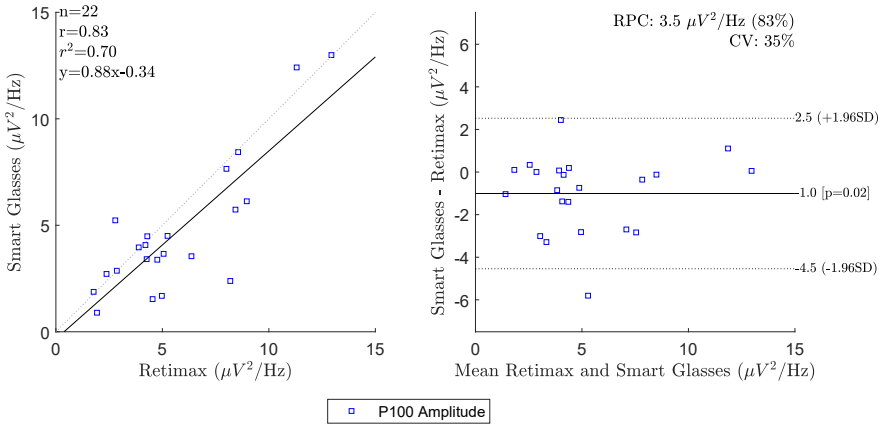

PR-VEP Comparison: Scatter Plot and Bland-Altman Plot, N135 Amplitude

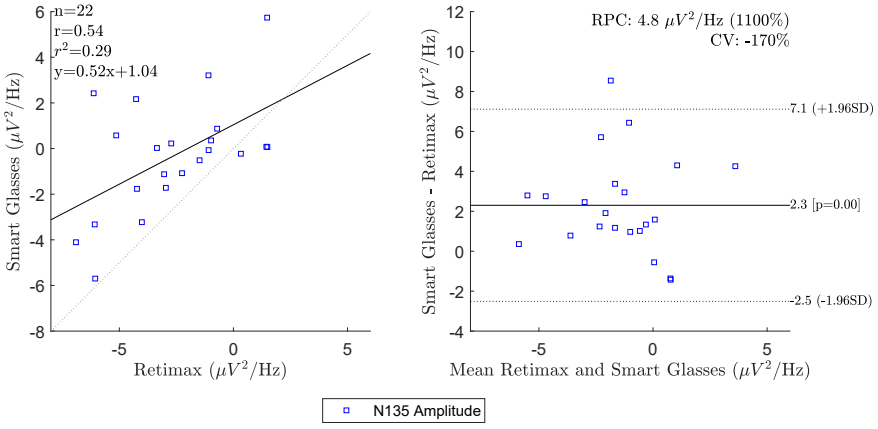

PR-VEP Comparison: Scatter Plot and Bland-Altman Plot, N75-P100 Amplitude

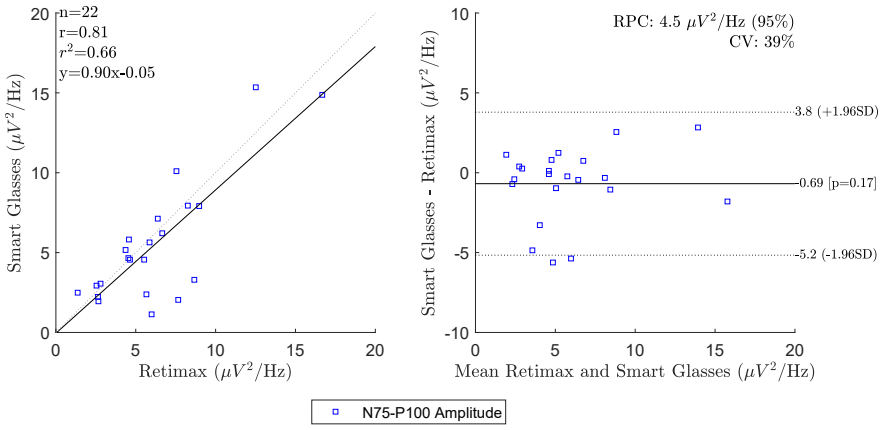

PR-VEP Comparison: Scatter Plot and Bland-Altman Plot, N135-P100 Amplitude

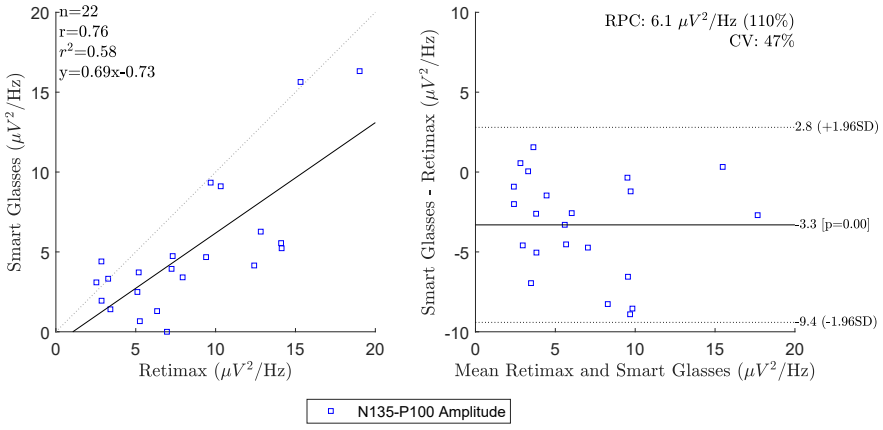

PR-VEP Comparison: Scatter Plot and Bland-Altman Plot, N75 Latency

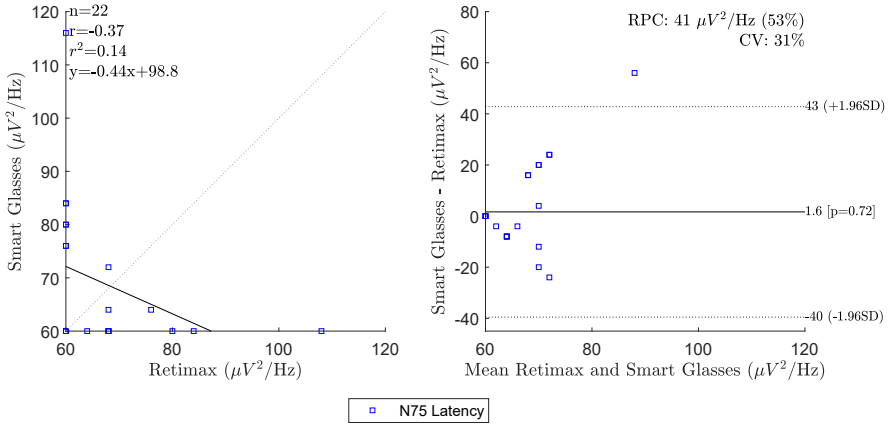

PR-VEP Comparison: Scatter Plot and Bland-Altman Plot, P100 Latency

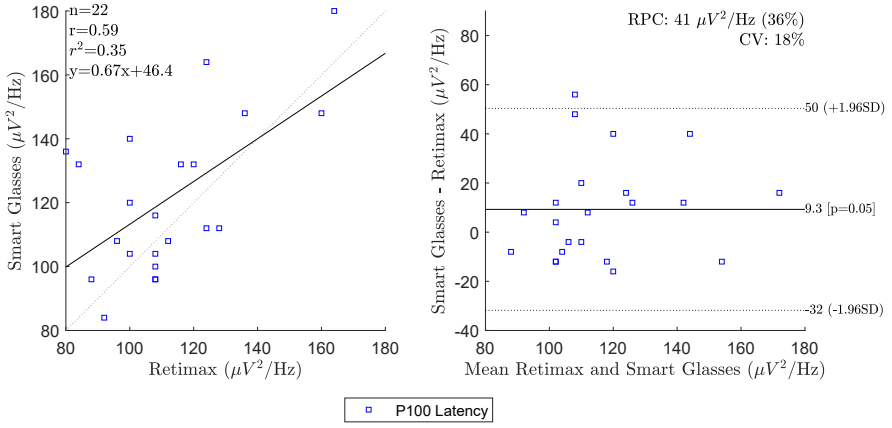

PR-VEP Comparison: Scatter Plot and Bland-Altman Plot, N135 Latency

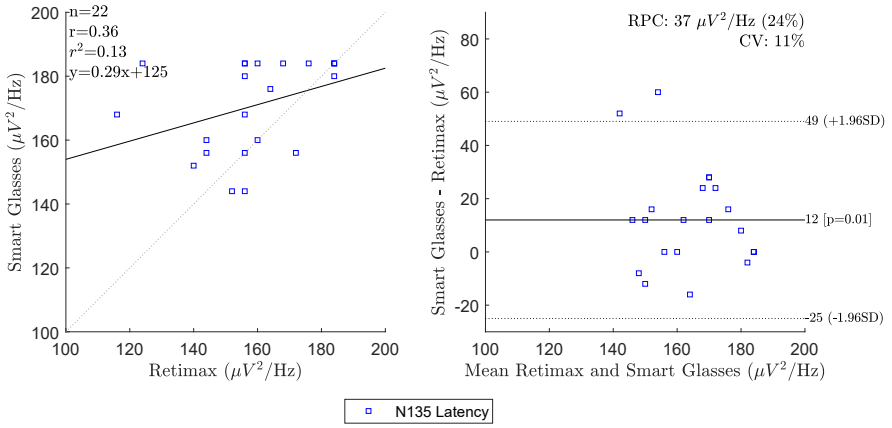

PR-VEP Comparison: Scatter Plot and Bland-Altman Plot, N75-P100 Latency

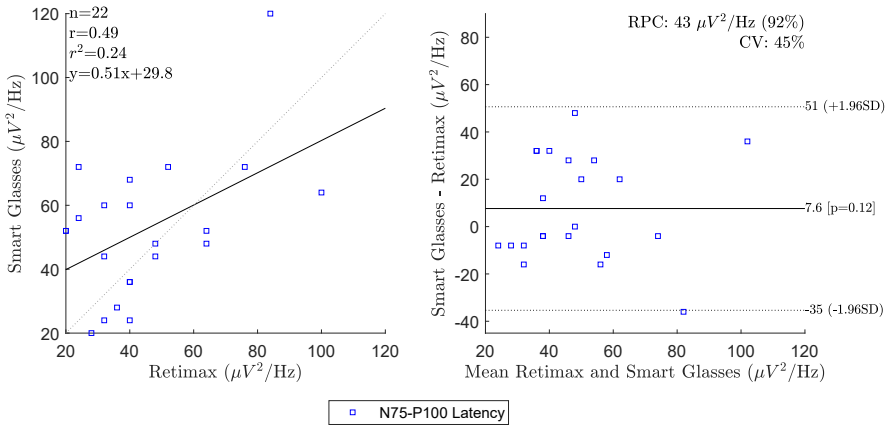

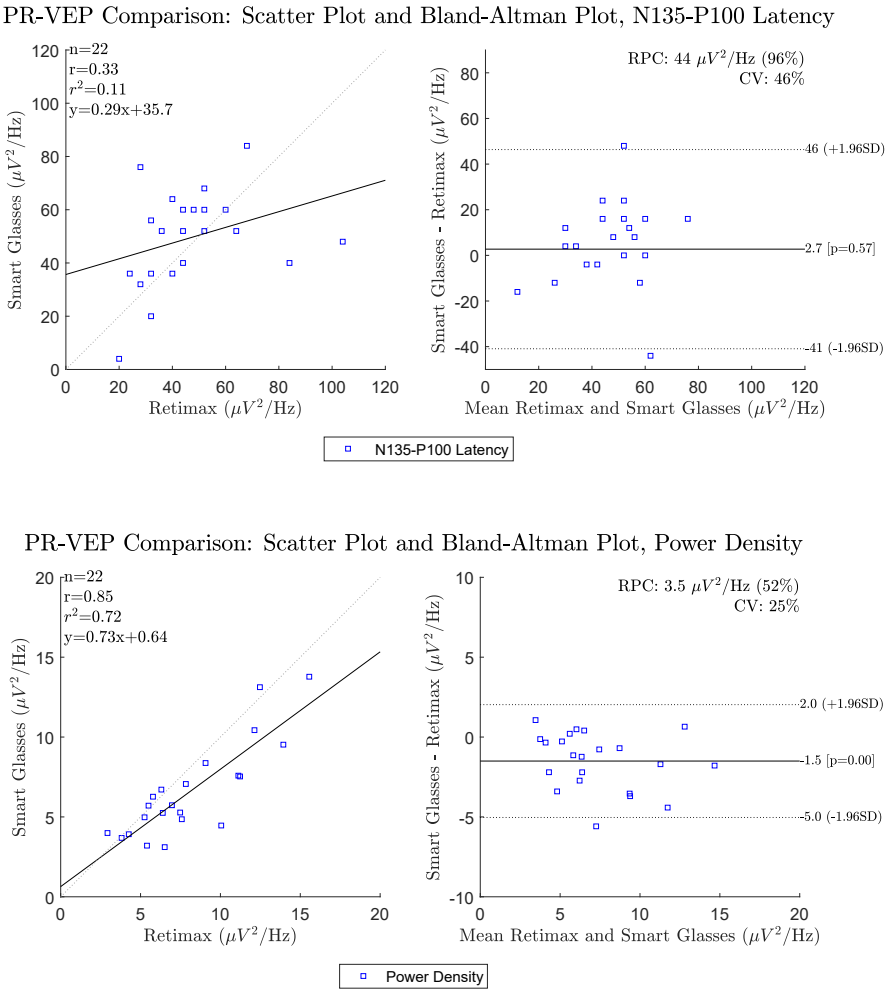

Figure 4.13: *Scatter plot and Bland-Altman plot of the ten features analyzed and of the power density for the pathologic subjects.*

Analyzing the results produced by the scatter plot, we can extract the following information: the best results we obtain with the amplitude of the P100 wave and with the relative amplitude N75-P100; both have a very strong correlation (Pearson r-value of 0.83 and 0.81 respectively) and the slope of the lines is respectively 0.88 and 0.90. We find the strongest correlation in the power density (Pearson r-value = 0.85) even if the slope of the line is slightly lower than the first two (0.73). Among the graphs we find another strong correlation in the case of the relative amplitude N135-P100 (Pearson r-value = 0.76 and slope of the line = 0.69), while 5 graphs on 11 show a

moderate correlation (0.33 < Pearson r-value < 0.59). The two worst results concern the amplitude and the latency of the N75 wave, characterized by a weak correlation and, in the case of latency, a negative slope of the line (Pearson r-value respectively of 0.08 and -0.37, slope of the lines of 0.06 and -0.44).

As for the Bland-Altman plot, in 7 out of 11 graphs it is possible to observe the same bias present in the case of healthy subjects: for low values in fact, Smart Glasses tend to overestimate the data obtained with the Retimax, while for higher values Retimax data tend to be underestimated.

Table 4.7: *Pathologic subjects, left eye: differences between Retimax and Smart glasses stimulations in terms of PR-VEP amplitudes and latencies. Values are presented as mean ± standard deviation. In the last row is also presented the power density of PR-VEP derived from both instruments. In the last column the absolute means difference are shown (AMD) and the relative decrease percentage.*

	Left Eye		
	Retimax	Smart Glasses	AMD
Amplitude (μV)			
N75 Amplitude	-0.09 ± 1.20	-0.87 ± 1.35	0.78 (89%)
P100 Amplitude	5.99 ± 2.77	4.87 ± 3.11	1.12 (18%)
N135 Amplitude	-2.19 ± 2.70	-0.11 ± 2.64	2.08 (94%)
N75-P100 Amplitude	6.08 ± 2.91	5.74 ± 4.04	0.34 (5%)
P100-N135 Amplitude	8.19 ± 4.12	4.99 ± 4.32	3.20 (39%)
Latency (ms)			
N75 Time To Peak	70.18 ± 14.23	62.55 ± 6.00	7.63 (10%)
P100 Time To Peak	112.00 ± 21.31	122.18 ± 25.57	10.18 (8%)
N135 Time To Peak	158.91 ± 19.10	166.55 ± 15.20	7.64 (4%)
N75-P100 Time To Peak	41.81 ± 17.19	59.63 ± 25.07	17.82 (29%)
P100-N135 Time To Peak	46.90 ± 18.25	44.36 ± 16.72	2.54 (5%)
Frequency Domain ($\mu V^2/Hz$)			
Power Density	8.21 ± 2.85	6.43 ± 2.97	1.78 (21%)

After that, a comparison was made between the average of the data obtained with the Retimax and the data obtained with the Smart Glasses; the difference in absolute value was calculated and was represented also in percentage terms. Even in this case, the left and right eye data have been separated to understand if there are any systematic errors in the stimulation of one of the two eyes (Tables 4.7 and 4.8).

Table 4.8: *Pathologic subjects, right eye: differences between Retimax and Smart glasses stimulations in terms of PR-VEP amplitudes and latencies. Values are presented as mean ± standard deviation. In the last row is also presented the power density of PR-VEP derived from both instruments. In the last column the absolute means difference are shown (AMD).*

	Right Eye		
	Retimax	Smart Glasses	AMD
Amplitude (μV)			
N75 Amplitude	-0.89 ± 1.83	-0.75 ± 1.11	0.14 (15%)
P100 Amplitude	5.44 ± 3.37	4.54 ± 3.43	0.90 (16%)
N135 Amplitude	-3.05 ± 2.51	-0.53 ± 2.47	2.52 (82%)
N75-P100 Amplitude	6.33 ± 4.15	5.29 ± 3.86	1.04 (16%)
P100-N135 Amplitude	8.49 ± 5.33	5.08 ± 4.36	3.41 (40%)
Latency (ms)			
N75 Time To Peak	64.36 ± 7.47	75.27 ± 16.66	10.91 (14%)
P100 Time To Peak	112.00 ± 2.84	120.36 ± 24.42	8.36 (6%)
N135 Time To Peak	158.54 ± 18.44	174.91 ± 13.27	16.36 (9%)
N75-P100 Time To Peak	47.63 ± 25.07	45.09 ± 16.59	2.54 (5%)
P100-N135 Time To Peak	46.54 ± 22.71	54.54 ± 18.87	8.00 (14%)
Frequency Domain ($\mu V^2/Hz$)			
Power Density	7.93 ± 4.06	6.70 ± 3.08	1.23 (15%)

Focusing on the amplitude of the left eye, we can observe a good ratio between the P100 amplitudes of the two devices (difference slightly higher than one μV, equal to 18% of the maximum value between the two averages)

and an excellent ratio between the relative amplitudes N75-P100, in which the Smart Glasses data differ from those of the Retimax only by 0.34 μV, for a decrease equal to 5%. From the absolute amplitudes of the two negative waves N75 and N135 we obtain instead bad results, due to the fact that, as regards many pathological subjects, their VEP is almost null, so the data is confused with the noise caused by artifacts. Instead, almost all the latencies show good results, with differences that oscillate between 4% and 10% (only the relative latency N75-P100 is different with a percentage difference of 29%). Finally, also the relationship between the power densities is very good (21% of decrease for the data of the Smart Glasses).

As regards the data obtained from the tests carried out on the right eyes, we can observe a similar trend to the other eye: good values of absolute mean difference for what concern the amplitude of the P100 wave and the relative amplitudes (the values of the data obtained with the Smart Glasses decreased respectively by 16%, 16% and 40%) and bad values regarding the amplitude of the N135 wave (82% difference). Good values in this case for the amplitude of the N75 wave, which undergoes a decrease of 15% as for the Smart Glasses. Even in this case, excellent result are obtained with the latencies of the waves: all of them oscillate between a 5% and a 14% of difference. Finally, also the ratio between the power densities is very good (15% of difference).

As a last analysis, the purely visual one was shown. For each test a morphological comparison was made, going overlapping the tracks obtained with the Retimax and Smart Glasses. The best VEPs, for both eyes, of all the patients, is presented below. Moreover, for each patient the ocular disease of which he is affected has been specified.

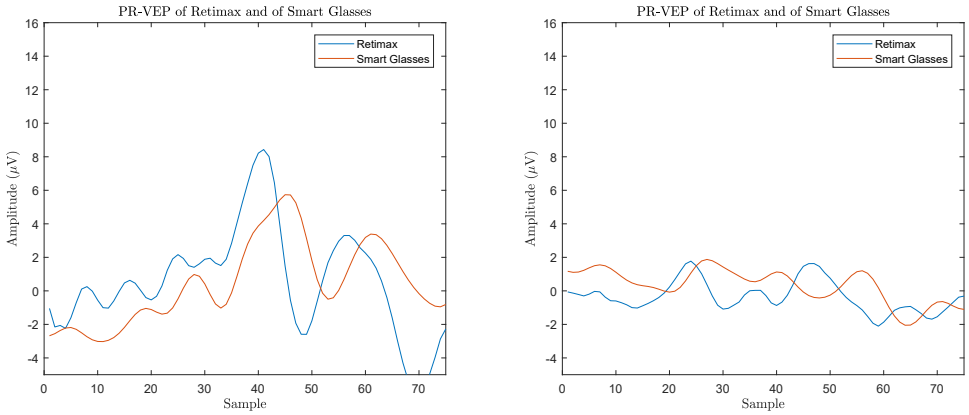

Figure 4.14: *Patient R.A.: on the left, the tracks of the left eye; on the right, the tracks of the right eye. The patient presents a Neovascular Corioretinopathy in the right eye and a Branch Retinal Vein Occlusion in the left eye.*

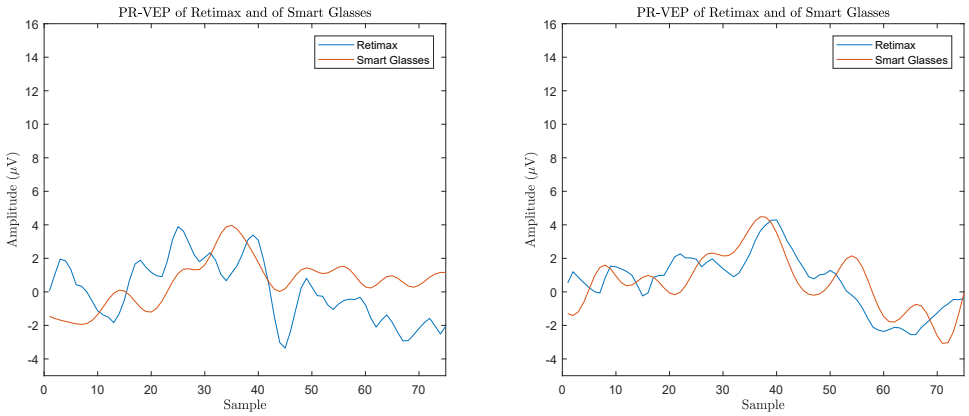

Figure 4.15: *Patient R.E.: on the left, the tracks of the left eye; on the right, the tracks of the right eye. The patient presents a Neovascular Corioretinopathy and a keratoconus in both eyes.*

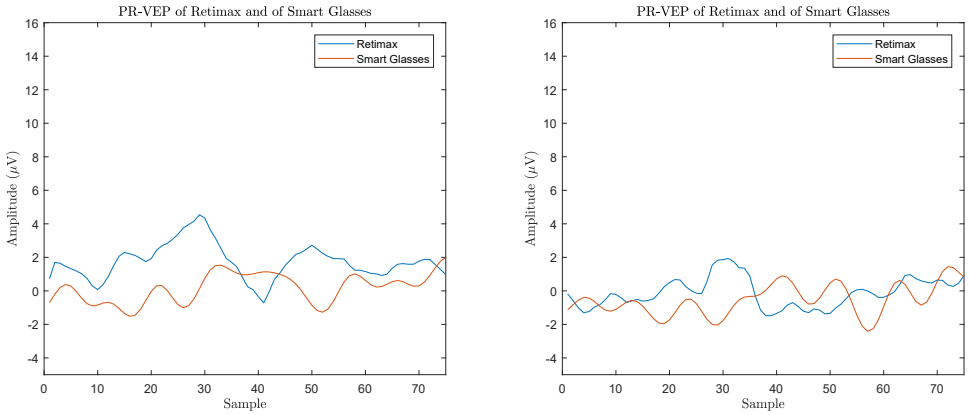

Figure 4.16: *Patient R.G.: on the left, the tracks of the left eye; on the right, the tracks of the right eye. The patient presents a Neovascular Corioretinopathy in both eyes with a disciform damage in the right eye.*

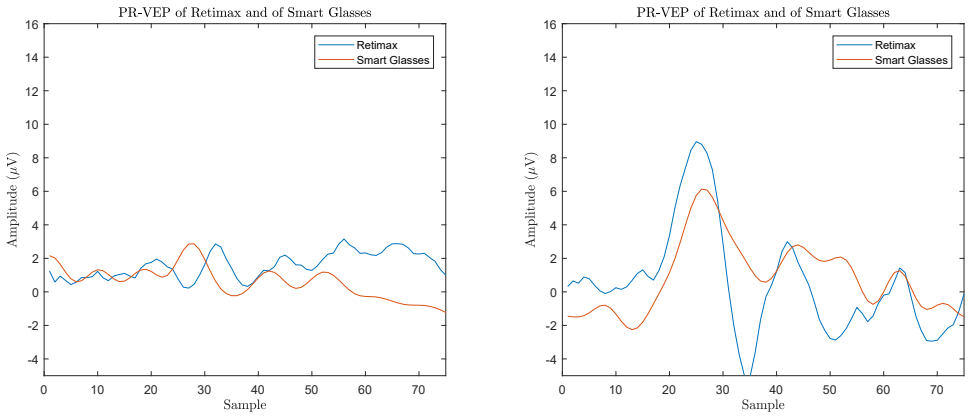

Figure 4.17: *Patient R.N.: on the left, the tracks of the left eye; on the right, the tracks of the right eye. The patient presents a Diabetic Macular Edema in both eyes with a chorioretinal atrophy in the left eye.*

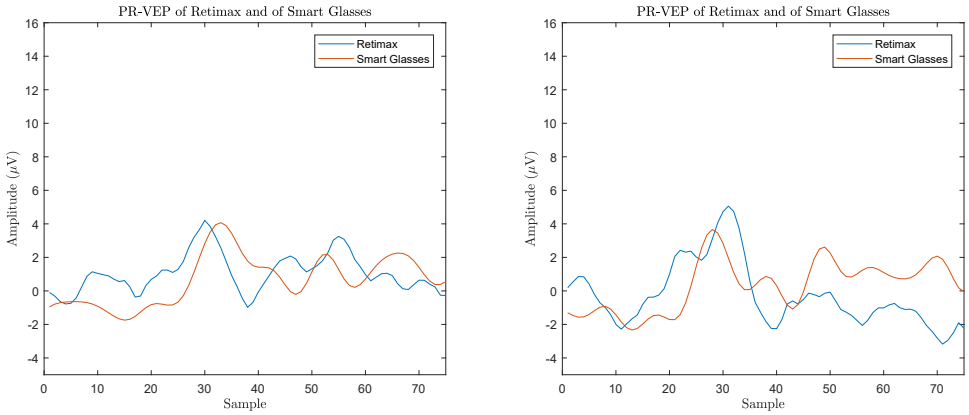

Figure 4.18: *Patient T.E.: on the left, the tracks of the left eye; on the right, the tracks of the right eye. The patient presents a Diabetic Retinitis in both eyes.*

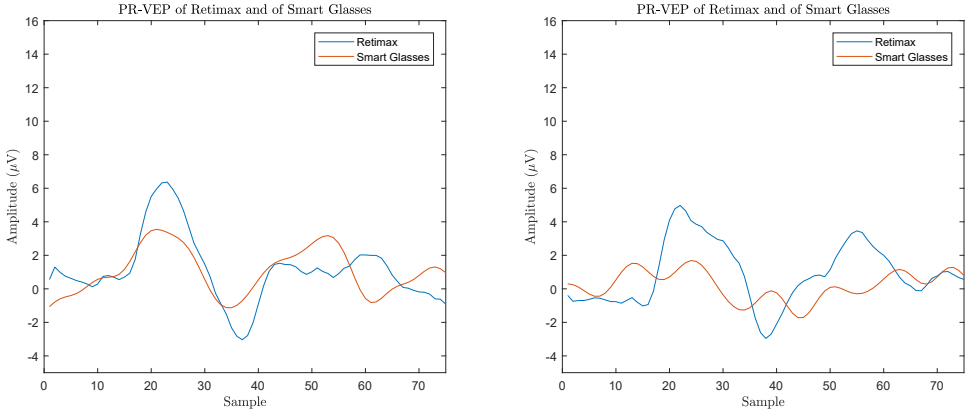

Figure 4.19: *Patient T.G.: on the left, the tracks of the left eye; on the right, the tracks of the right eye. The patient presents a Cistoid Macular Edema with Subatrophy of Pigmented Epithelium in the right eye.*

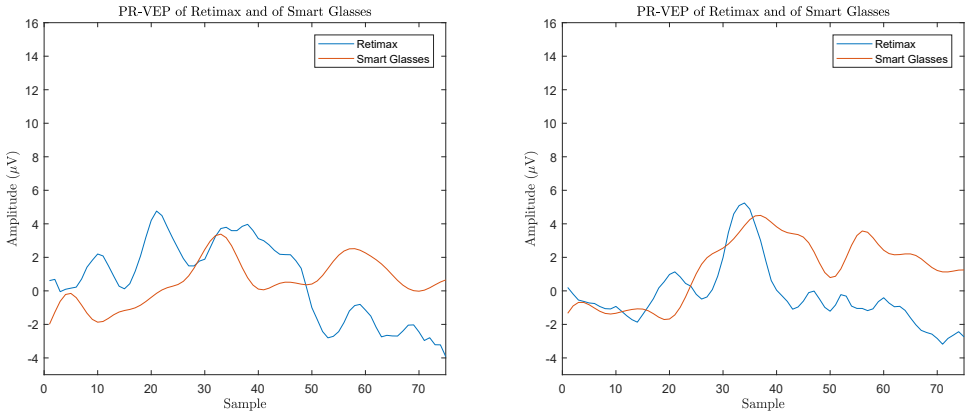

Figure 4.20: *Patient T.G.P.: on the left, the tracks of the left eye; on the right, the tracks of the right eye. The patient presents a Myopic Neovascular Corioretinopathy in both eyes.*

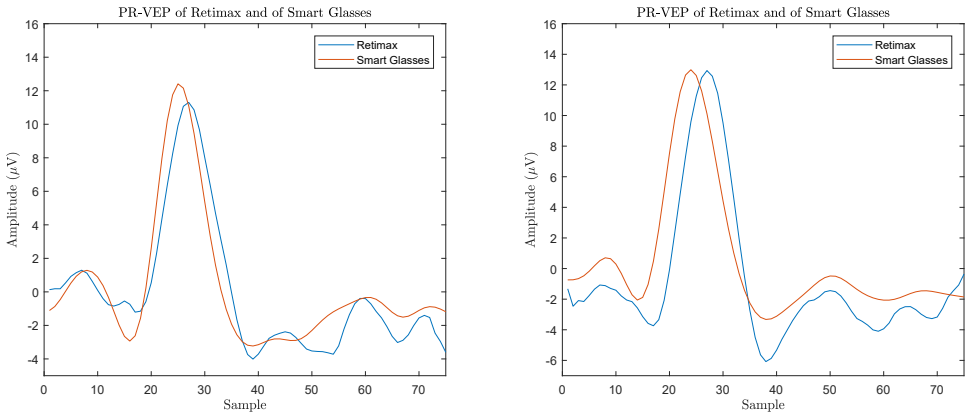

Figure 4.21: *Patient T.L.: on the left, the tracks of the left eye; on the right, the tracks of the right eye. The patient presents a Diabetic Macular Edema in both eyes. Currently being treated with anti-VEGF.*

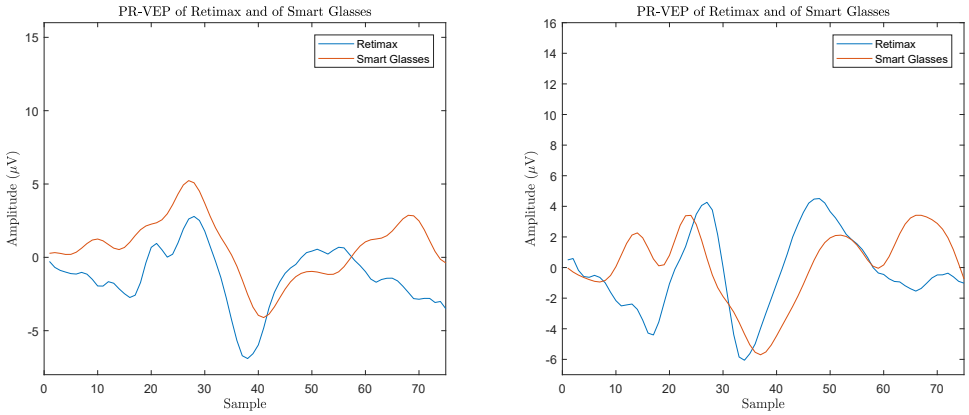

Figure 4.22: *Patient V.M.: on the left, the tracks of the left eye; on the right, the tracks of the right eye. The patient presents an Active Neovascular Corioretinopathy in both eyes.*

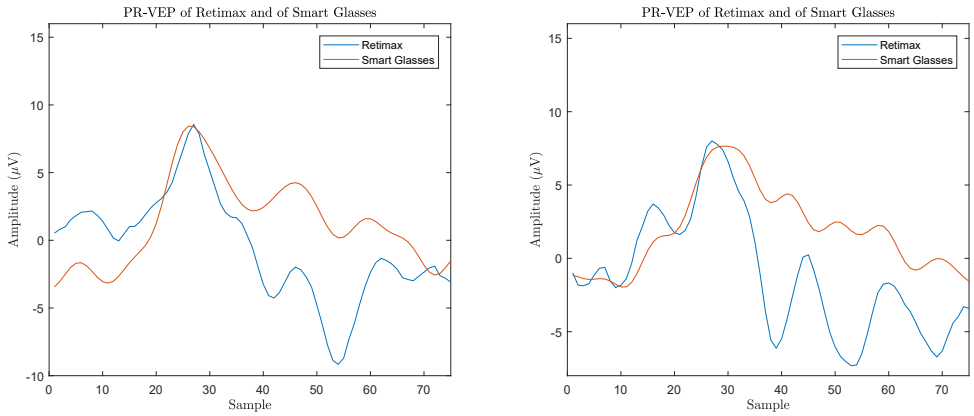

Figure 4.23: *Patient V.M.A.: on the left, the tracks of the left eye; on the right, the tracks of the right eye. The patient presents a Diabetic Macular Edema in both eyes.*

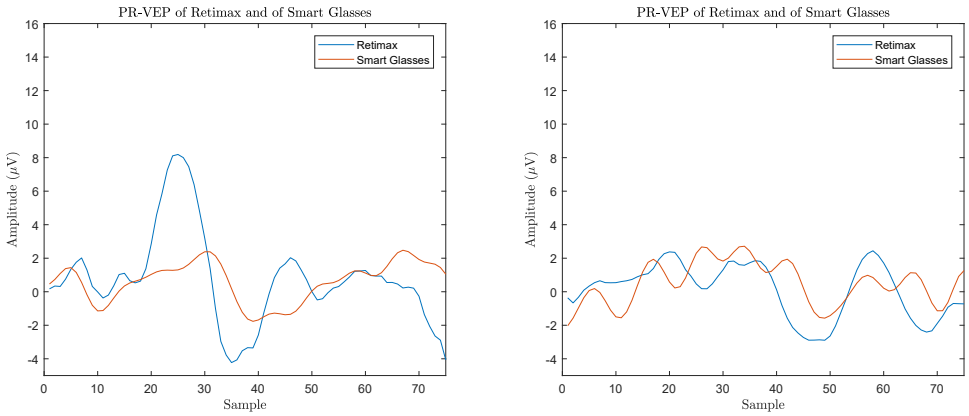

Figure 4.24: *Patient V.R.: on the left, the tracks of the left eye; on the right, the tracks of the right eye. The patient presents a Neovascular Corioretinopathy in both eyes with a disciform damage in the right eye.*

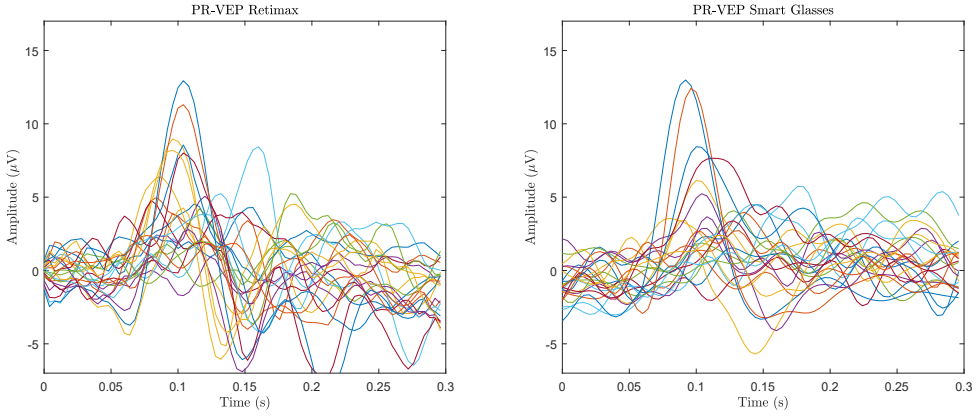

Figure 4.25: *All the PR-VEP waveforms obtained during the test, using the Retimax (a) and the smart glasses (b).*

In 19 graphs on 22 the tracks are comparable and consequently show a satisfying result. 6 traces are almost null, due to the ocular pathology of which the patients are affected; therefore what is observed is only noise caused by luminous artefacts.

Chapter 5

Conclusion and Future Works

We proposed an integrated, low cost portable solution for pattern reversal visual evoked potential tests. The system is able to generate visual stimuli such as the commonly used chessboard, with the possibility to choose different parameters (spatial and/or temporal frequency). The resulting PR-VEPs are acquired in real time by a commercial EEG acquisition board (OpenBCI® Cyton board) following the 10/20 International System for the positioning of the electrodes. Data is then sent to a laptop via Bluetooth connection through an OpenBCI dongle and processed in MATLAB®.

The advantages of our device are remarkable: the exam can be executed also to bedridden or movement impaired patients; its portability can enable PR-VEPs exams at patient's home and not last the low cost (a price estimation of the prototype device is about 1,200 €, while the current commercial value of a standard PR-VEPs instrumentation ranges from 20,000 to 70,000 €).

In order to evaluate the performance of our device, first acquisitions of 20 healthy eyes were performed, to better calibrate the device; subsequently the system was tested on 22 pathological eyes to verify correct functioning even under partially-sight conditions.
The results of our device were compared with those of the commercial PR-VEPs exam device (Retimax® CSO), using statistical analysis algorithms

such as the Kolmogorov-Smirnov test to verify the normality of the data, the scatter plot to understand if the relationship between the two databases was linear, the Bland-Altman plot to detect any bias or systematic errors in the system. Subsequently, for each of the ten main characteristics, values relative to the absolute difference between the averages calculated for both devices were extracted. Finally, a visual evaluation was made by plotting the tracks of Retimax and Smart Glasses on the same graph.

Although this is a preliminary assessment and therefore the samples analyzed are few, we can still see a strong similarity between the results of the two instruments, in terms of amplitudes and latencies of the three characterizing waves. In the case of pathological subjects the tracks show some differences: this is due to the low amplitude (sometimes absent) of the waves, which are confused with the random noise. Therefore, these differences are negligible for the purpose of the evaluation of the good propagation of the signal through the optical pathways.

As a matter of fact, we are persuaded that this device could be a good diagnostic instrument in ophtalmology.

Future development of our project:

- the use of the MATLAB® interface will be eliminated, in order to allow everyone to use it without having to buy a license;
- the database in which the 20 combinations of spatial and temporal frequencies are present will be enriched, adding the possibility to change also other stimulus parameters;
- a further stimulus modalities (Flash VEP and Onset/Offset pattern VEP) might be introduced and a real time analysis of the patient's ocular movement will be implemented, interrupting the stimulation when the patient no longer looks at the center of the chessboard and resumes once he returns to the conditions ideal stimulus;

- a new model of Smart Glasses will be tested, more comfortable and more stable than the current one. Moreover, thanks to the structure of the new model, a dark room will no longer be necessary because the patient will already be well isolated from the outside world;
- the device will be tested on a larger number of subjects in order to evaluate its funcionality on a large scale.

Aknowledgment

In questa sezione desidero esprimere la mia gratitudine nei confronti di tutte le persone che mi hanno accompagnato lungo questo percorso e che mi hanno aiutato nella stesura della tesi, con suggerimenti e critiche costruttive.

Ringrazio anzitutto il prof. Danilo Demarchi, Relatore, per avermi dato la possibilità di lavorare su questo progetto. Il suo supporto è stato fondamentale, dal punto di vista lavorativo ma soprattutto umano, un pregio che al giorno d'oggi in pochi possono vantare.
Proseguo con l'Ing. Alessandro Sanginario, Co-Relatore, il quale, oltre ad avermi fornito un enorme aiuto durante questo cammino, si è sempre rivolto nei miei confronti come un amico.
Vorrei poi ringraziare i Dottori del centro oftalmico Sperino, Lorenzo Canavese e Davide Putignano, per la loro disponibilità nel fornirmi tutta la strumentazione e la conoscenza medica di cui necessitavo.
Uno dei miei ringraziamenti più grandi va a Rossana, da cui ho ereditato il progetto, per la sua infinità disponibilità: il suo aiuto è un gesto che non dimenticherò. Un ringraziamento va anche a Fabio, Andrea e Sofia, i quali hanno reso il laboratorio "Civera" una sede in cui lavorare col sorriso e a tutti i miei amici/colleghi con i quali ho avuto a che fare in questo percorso di laurea.

Ultimi nell'elenco, ma primi per importanza, ringrazio la mia famiglia, per avermi dato la possibilità di raggiungere questo traguardo e Diletta, per avermi aiutato, supportato e sopportato in tutti questi anni.
Questo lavoro è dedicato a loro.

Bibliography

[1] Terracciano R. *Pattern-Reversal Visual Potential Evoked by Android Application on Smart Glasses: prototyping, analysis of the stimulation and aquisition system.* 2017.

[2] Anatomy of the eye. `http://www.eyerisvision.com/anatomy-of-the-eye.html`.

[3] The retina: Where vision begins. `http://www.eyerisvision.com/anatomy-of-the-eye.html`.

[4] The crayola-fication of the world: How we gave colors names, and it messed with our brains. `http://aminotes.tumblr.com/post/25518386232/the-crayola-fication-of-the-world-how-we-gave`.

[5] Bach M. Electrophysiological approaches for early detection of glaucoma. *European journal of ophthalmology*, 11, 2001.

[6] Odom J.V., Bach M., Barber C., Brigell M., Marmor M.F., Tormene A.P., and Holder G.E. Visual evoked potentials standard. *Documenta ophthalmologica*, 108, 2004.

[7] Odom J.V., Bach M., Brigell M.G., Holder G.E., Mcculloch D.L., Mizota A., and Tormene A.P. Iscev standard for clinical visual evoked potentials: (2016 update). *Documenta Ophthalmologica*, 2009.

[8] Epson moverio bt-200. `https://www.epson.it/products/see-through-mobile-viewer/moverio-bt-200`.

[9] Openbci cyton biosensing board. `https://shop.openbci.com/products/cyton-biosensing-board-8-channel?variant=38958638542`.

[10] Garduer E.P. and Martin J.H. *La codificazione delle informazioni sensoriali*. Casa Editrice Ambrosiana, 2003.

[11] Oyster C.W. and Haver N. *The human eye: structure and function*, volume 766. Sinauer Associates Sunderland, MA, 1999.

[12] Marieb E.N. and Hoehn K. *Human anatomy & physiology*. Pearson Education, 2007.

[13] Kolb H. The architecture of functional neural circuits in the vertebrate retina. the proctor lecture. *Investigative ophthalmology & visual science*, 35, 1994.

[14] Dowling J.E. and Boycott B.B. Organization of the primate retina: electron microscopy. *Proc. R. Soc. Lond. B*, 166, 1966.

[15] Mason C., Kandel E.R., Schwartz J.H., and Jessel T.M. Le vie visive centrali. *Principi di neuroscienze. Seconda edizione. Ambrosiana. Milano*, 1991.

[16] Kandel E.R., Schwartz J.H., Jessell T.M., Siegelbaum S.A., Hudspeth A.J., Perri V., and Spidalieri G. Principi di neuroscienze. 1994.

[17] Brindley G.S. Physiology of the retina and the visual pathway. 1960.

[18] Ferrarese C., Appollonio I., Cavaletti G., Sganzeria E.P., Cortelli P., Federico A., and Marciani M.G. *Malattie del sistema nervoso*. McGraw-Hill, 2011.

[19] Parisi V. and Coppola G. Elettrofisiologia oculare.

[20] Arden G.B. and Bankes J.L. Foveal electroretinogram as a clinical test. *The British journal of ophthalmology*, 50, 1966.

[21] Hood D.C., Bach M., Brigell M., Keating D., Kondo M., Lyons J.S., Marmor M.F., McCulloch D.L., Palmowski-Wolfe A.M., and Anja M. Iscev standard for clinical multifocal electroretinography (mferg). *Documenta Ophthalmologica*, 124, 2012.

[22] Bach M., Brigell M.G., Hawlina M., Holder G.E., Johnson M.A., McCulloch D.L., Meigen T., and Viswanathan S. Iscev standard for clinical pattern electroretinography (perg): 2012 update. *Documenta Ophthalmologica*, 126, 2013.

[23] Nakamura A., Kakigi R., Hoshiyama M., Koyama S., Kitamura Y., and Shimojo M. Visual evoked cortical magnetic fields to pattern reversal stimulation. *Cognitive Brain Research*, 6, 1997.

[24] Barlow H.B. Possible principles underlying the transformations of sensory messages. 1961.

[25] Pescosolido N. and Stefanucci A. *Elettrofisiologia clinica e basi fisiologiche della visione*. Fabiano Canelli, Italia, 2011.

[26] Retimax cso. `http://www.optomedica.com/prodotti/diagnostica/elettrofisiologia/cso-retimax-advanced/`.

[27] Nuprep eeg & ecg skin prep gel. `https://bio-medical.com/nuprep-eegecg-skin-prep-gel-3-pack-of-4oz-tubes.html`.

[28] Gold electrodes skin-cup for eeg. `http://www.medicalexpo.fr/prod/gaes/product-81252-684870.html`.

[29] Konix eeg paste. `https://www.elettromedicali.it`.

[30] Cosenza F. *Realtà aumentata per dispositivi android: lo stato dell'arte*. PhD thesis.

[31] Klem G.H., LuÈders H.O., Jasper H.H., and Elger C. The ten-twenty electrode system of the international federation. *Electroencephalogr Clin Neurophysiol*, 52, 1999.

[32] Wikipedia. Test di kolmogorov-smirnov, 2018. [Online; in data 19-giugno-2018].

[33] Hsu H. and Lachenbruch P.A. Paired t test. *Wiley Encyclopedia of Clinical Trials*, 2008.

[34] Myles P.S. and Cui J. Using the bland–altman method to measure agreement with repeated measures, 2007.

[35] Wikipedia contributors. Scatter plot, 2018. [Online; accessed 8-June-2018].

[36] Belloni S. Degenerazione maculare senile. 2010.

[37] Rabb M. F., Garoon I., and La Franco F. P. Myopic macular degeneration. *International ophthalmology clinics*, 1981.

[38] Antcliff R.J. and Marshall J. The pathogenesis of edema in diabetic maculopathy. *Seminars in ophthalmology*, 1999.

[39] Badalà F. The treatment of branch retinal vein occlusion with bevacizumab. *Current opinion in Ophtalmology*, 2008.

[40] Spaide R.F., Laud K., Fine H.F., James M Klancnik J.R., Meyerle C.B., Yannuzzi L.A., Sorenson J., Slakter J., Fisher Y.L., and Cooney M.J. Intravitreal bevacizumab treatment of choroidal neovascularization secondary to age-related macular degeneration. *Retina*, 2006.